CAIT-UTC-NC34

Installation of Embedded Accelerometers in Precast Girders for Nibley Utah Bridge

FINAL REPORT
August 2018

Submitted by:

Tyson Scott Alder
Graduate Student, USU

Marvin W. Halling
Professor, USU

Paul J. Barr
Professor, USU

Utah State University
4110 Old Main Hill
Logan, UT 84332

External Project Manager

Shaun Dustin
Engineering Manager
Campbell Scientific, Inc.

In cooperation with

Rutgers, The State University of New Jersey
and
Bridge Diagnostic Instruments
and
U.S. Department of Transportation
Federal Highway Administration

Disclaimer Statement

The contents of this report reflect the views of the authors, who are responsible for the facts and the accuracy of the information presented herein. This document is disseminated under the sponsorship of the Department of Transportation, University Transportation Centers Program, in the interest of information exchange. The U.S. Government assumes no liability for the contents or use thereof.

The Center for Advanced Infrastructure and Transportation (CAIT) is a National UTC Consortium led by Rutgers, The State University of New Jersey. Members of the consortium are the University of Delaware, Utah State University, Columbia University, New Jersey Institute of Technology, Princeton University, University of Texas at El Paso, Virginia Polytechnic Institute and the University of South Florida. The Center is funded by the U.S.

TECHNICAL REPORT STANDARD TITLE PAGE

1. Report No.	2. Government Accession No.	3. Recipient's Catalog No.
CAIT-UTC-NC34		

4. Title and Subtitle	5. Report Date
Installation of Embedded Accelerometers in Precast Girders for Nibley Utah Bridge	August 2018
	6. Performing Organization Code CAIT/Utah State University
7. Author(s) Tyson Scott Alder, Marvin W. Halling, Paul J. Barr	8. Performing Organization Report No. CAIT-UTC-NC34
9. Performing Organization Name and Address Utah State University 4110 Old Main Hill	10. Work Unit No.
	11. Contract or Grant No. DTRT13-G-UTC28
12. Sponsoring Agency Name and Address Center for Advanced Infrastructure and Transportation Rutgers, The State University of New Jersey 100 Brett Road, Piscataway, NJ 08854	13. Type of Report and Period Covered Final Report 04/01/16 to 08/31/17
	14. Sponsoring Agency Code

15. Supplementary Notes
U.S. Department of Transportation/Research and Innovative Technology Administration
1200 New Jersey Avenue, SE, Washington, DC 20590-0001

16. Abstract

Dynamic monitoring of structures is a method of detecting changes and damage to the structure. Vibration based monitoring has been used to detect damage in rotating machinery and is gaining popularity in the field of Structural Health Monitoring (SHM). Monitoring involves detecting changes in natural frequencies and changes in mode shapes. These changes reflect changes to properties of the bridge which can indicate damage.

The Nibley Bridge is a single span bridge comprised of ten deck bulb girders. The bridge spans 25.91 m (85 ft) and includes two lanes, sidewalks on both sides, and a small median. The Nibley Bridge was constructed with monitoring in mind. A dynamic monitoring system was planned to detect frequencies for long term monitoring. Initial monitoring of the embedded accelerometers was ineffective, so additional testing was required. An impact test was done with additional sensors to calibrate the embedded sensors. To further define the natural frequencies and mode shapes of the bridge, two shaker tests were also performed.

The embedded sensors were noted as having a large noise range. Also, they required a specific datalogger to detect meaningful data. Recommendations for the use of the embedded accelerometers were determined and defined. The additional tests were able to assist in calibrating the accelerometers as well as defining the natural frequencies and mode shapes of the structure. Natural frequencies were defined for each test and the changing condition of the bridge between those tests. The addition of asphalt occurred between two tests and a change of approximately 20°C between the other two tests. Though there is not much information to form a correlation, the detected changes define the dynamic aspects of the bridge.

Lastly, mode shapes were determined and a Modal Assurance Criterion (MAC) analysis was done to correlate the measured and analytical mode shapes. This model helped to indicate which parameters effect the mode shapes of the structure. Comparison between these parameters and changes between them help to indicate the predicted behavior of the structure under different circumstances. Though these tests do not define all of the dynamic properties of the bridge, they do provide a general baseline of values that can be expected for future tests of the structure.

17. Key Words	18. Distribution Statement
Embedded accelerometers, Structural Health Monitoring, damage detection, ambient vibration	

19. Security Classification (of this report)	20. Security Classification (of this page)	21. No. of Pages	22. Price
Unclassified	Unclassified	89	

Form DOT F 1700.7 (8-69)

Table of Contents

List of Figures

List of Tables

Chapter 1: Introduction and Literature Review

Structural Health Monitoring (SHM) is the practice of inspecting structures to determine if there is damage. Inspections are typically done visually, but research over the past few decades has been focused on establishing methods to detect damage using properties detected by instruments. In this way damage can be identified more thoroughly than by visual inspection alone. Certain sensors, like strain gauges, can detect localized damage, while measuring the dynamic properties of a structure has the potential to detect global damage. These concepts have been used for testing mechanical systems in controlled environments but have additional difficulty accounting for the environmental effects on structures in the field (Sohn H. 2007). Much of the current research is focused on mitigating operational effects in order to clearly identify if damage has occurred. A particular focus is on bridges, which make up a large portion of existing infrastructure and often experience loads beyond those expected.

The dynamic properties of an object relate to vibrations caused when the object is excited by a force. All objects have a natural vibration based on various factors like their length and stiffness. The rate that this vibration occurs is called the natural frequency. Because objects can vibrate in more than one way, there are multiple natural frequencies for each vibration shape. A jump rope, for example, is typically swung to create a large central loop. Swinging the rope faster will create a sideways figure 8 in the center. These are the first two mode shapes of the jump rope, and each has a specific frequency at which it occurs. In each structure, multiple mode shapes and frequencies can be detected. When damage occurs, the structural stiffness is likely to decrease, and the natural frequency will change. By noting the change in frequency, it can be determined that the structure has experienced damage.

Other factors affect the natural frequencies of structures. Environmental factors such as temperature, wind, boundary conditions, and others have been observed to change the natural frequency beyond that which is expected by damage (Zhou and Yi 2014). Temperature typically has a large influence on the natural frequency. Many studies and multiple methods have been used to correlate and mitigate the frequency changes caused by temperature. However, because each structure is completely unique, the methods have been difficult to apply overall. Primarily, research has focused on bridges. The general method is to establish a baseline frequency of the undamaged structure. To mitigate temperature or other effects, the baseline should exist over an extended period of time and conditions. After establishing a baseline of frequencies and mode shapes, deviations from these values are expected to be caused by damage. Though detecting damage is still a subject of further review, establishing a baseline is the first step required for any analysis.

The goal of this study is to establish a baseline for the recently constructed Nibley Bridge. Embedded and external sensors were used as well as a variety of excitation techniques to determine natural frequencies and mode shapes. Embedded thermocouples were used to extract internal temperature measurements of the structure. Embedded accelerometers were used in conjunction with external velocity transducers to establish the natural frequencies occurring on the bridge. Using this baseline, future tests can be done to ascertain the properties of the bridge over time.

Literature Review

A review of literature relating to the overarching subject of SHM as well as aspects that particularly relate to this project was undertaken to gain a thorough background on the subject.

Following is a selection of what were deemed to be the most pertinent articles. The review is split into five sections, each one focusing primarily on the results of a specific article.

Long Term Bridge Monitoring

A long term study done by Peeters documents the effects of temperature and damage on the Z-24 Bridge in Switzerland (Peeters et al. 2000). Multiple methods of bridge excitation are used, including ambient, impact, and shaker excitation. The methods are compared to show their effectiveness in determining modal frequencies. The Z-24 Bridge was monitored for nearly a year before artificial damage was incurred. The goal was to determine the difference in frequency between damage and natural effects like temperature, as well as evaluate methods to determine those changes. Damage was successfully detected when compared to the frequencies obtained by long term ambient monitoring. The success of this project demonstrates the use of frequency monitoring for SHM.

Three excitation sources were used in the monitoring of the bridge: two shakers, a drop weight, and ambient excitation. Measurements for each source were recorded as damage was inflicted on the bridge as part of reconstruction. Prior to damage, modal frequencies were determined using each excitation source for the first six modes of the bridge. The determined frequencies aligned best for lower modes, with increasing divergence at higher mode shapes. Only those shapes below 30 Hz were detected. Each method of monitoring was compared to indicate the strengths and weaknesses of each. Shaking the bridge was effective for detecting modes occurring above frequencies of 1 Hz. The other drawback of shaker testing indicated by the study is the cost to obtain and use the shakers. The shaker input was a noise signal ranging from 3 Hz to 30 Hz, similar to the ambient condition. In comparison, ambient excitation is

naturally the cheapest option, and is the only method that can be used for continuous monitoring. Ambient monitoring had difficulties detecting higher frequency modes, as these modes were excited less by ambient forces. Mode shapes were developed using data from each of the excitation methods. The mode shapes and frequencies were similar for the first five modes, with the shaker test detecting a different sixth mode.

Prior to the damage incursion, continual monitoring of the bridge occurred for 10 months. Monitoring was done primarily to detect changes in the dynamic properties of the structure due to environmental effects. Sensors monitored air and concrete temperature, humidity, expansion, and other factors. Only the first four modes were focused on as part of the data, likely because fewer accelerometers were used. These modes showed bilinear behavior relative to temperature, intersecting at zero degrees Celsius. Below zero, the frequency slope increases steeply. The added stiffness is assumed to come from the asphalt. When the asphalt is frozen, it adds considerable stiffness to the structure but does not contribute above freezing. It is also noticeable that the spread between frequencies below subzero temperatures is much tighter than those above freezing.

To model the bridge, a Black Box method was used. Temperature affects the natural frequencies in multiple ways that may be different for each structure. Rather than account for all the possible effects of temperature, collected values of temperature and frequency are used to calibrate a model to match these values. While linear regression is typically used to model a linear relationship, thermal dynamics were noted on the bridge that would not follow the linear analysis. Certain portions of the bridge would heat at different rates due to differing material in the bridge. Thus, dynamic modeling was used to describe the temperature changes of the bridge. Based on the model, new frequencies could be compared to those predicted by the model. The

Z-24 Bridge was modeled and then compared to the measured values throughout the year before damage occurred to the bridge. The damage was noted as a drop in frequency occurring when damage was inflicted on the structure.

This paper describes the value in establishing a structural model for comparison tests. In order to detect damage, each structure must be individually measured to establish a baseline condition. After this value is established, future damage detection can be determined by comparing current conditions with the healthy structure condition. Damage was successfully detected in this case, validating the methods used.

Comparison of Environmental Factors

Sohn (2007) compiled a literary review of structural health monitoring and its progression over time, as well as efforts made to negate environmental effects on the monitoring of structures. While methods for SHM on mechanical systems have been in existence for some time, it is difficult to move those monitoring methods out of the lab and into the field. Often structures in the field have many effects that cannot be accurately taken into account, and therefore further experiments in the field are required. These variations are caused by environmental effects. Temperature, boundary conditions, wind, and loading effects are examined here.

Temperature effects on a dynamic response have been the subject of many studies and observation. It has been noted that expansion of asphalt on a bridge can change the natural frequencies of a bridge, and this expansion likewise changes the condition at the boundaries. Frequency changes have also been observed through temporal temperature changes. Changes in

frequency have been shown to vary from 5% over the day to 10% over the year. Thermal stresses have been shown to have the largest impact on frequency of all ambient factors.

Boundary conditions can affect natural frequencies much more than damage can. While a boundary change can occur due to damage, boundary changes typically accompany material changes due to temperature. It has been found that freezing of a bridge's supports cause much higher frequency changes than those caused by damage. It is also notably difficult to determine the boundary conditions of a structure, making this measurement difficult to discern.

Research on the effect of mass loading on modal parameters has indicated that the effect is relative to the loading and mass of the structure. Shorter bridges are affected more by heavy traffic loading; however, no effect is observed for longer bridges. While the expected mass loading should be considered in monitoring a bridge, it has not been seen to have a large impact on frequency.

Wind loads on long span bridges can cause vibration. Energy from wind vibration can become larger than the dampening effect, causing fluttering. This has been shown to change the lower fundamental frequencies of the bridge. It also affects the dampening ratio of a bridge depending on the wind speed and vibration amplitude. These wind vibrations have the greatest effect on cable stayed bridges.

In order to discern damage features from naturally occurring ones, multiple data normalization methods have been used by researchers. A primary method uses linear regression analysis. This requires that a correlation be found between multiple variables, such as frequency and temperature, and then be used as a baseline for an undamaged structure. Because damage would affect the frequency in the same manner temperature would, the temperature and frequency must both be monitored or damage could not be detected. This paper provides an

overview of progress made towards long term structural health monitoring using dynamic methods.

Damage Effects on Frequency

A study by Hsieh details the application of vibration based structural health monitoring on multiple projects done using various excitation techniques (Hsieh et al. 2006). These techniques are valuable for detecting damage that occurs on the subsurface. The common method of visual inspection can detect surface corrosion or other indicators but cannot detect internal flaws that may have occurred. Structural health monitoring has the potential to detect internal damage and supplement visual inspection (Aggour and Fouad 1991). Vibrational properties can be excited using multiple methods, typically ambient and forced vibration. Free vibration, that caused by releasing a structure from a displaced position, occurs at natural frequencies. The identified natural frequencies can be monitored and can reflect damage.

Multiple studies are mentioned in the paper detailing the use of this type of structural health monitoring. Three case studies are mentioned in greater detail which describe multiple uses of these techniques. The first example used long term monitoring of ambient vibration to detect frequency measurements of the bridge. Long term monitoring was done for nearly 3 years before a forced vibration test was done. The forced vibration test included additional velocity transducers placed in the vertical position. The differences between the detected frequencies are compared throughout the year. Modal frequencies were detected, with only minor differences between the frequencies of the modes. In comparing all tests, the largest difference was 8.3% on Mode 1. This indicates that while frequency changes may be minimal, differences between frequencies tend to be larger in the lower modes of the structure.

The next test demonstrates the effect of damage on a structure. The South Temple Bridge was subject to forced vibration during various damage conditions. Damage was consecutively inflicted and then repaired to detect the changing stiffness of the structure. Damage occurred at the bents and the excitation occurred in the horizontal position. A finite element model was made to correlate the measured frequencies with the model. The finite element model was adjusted to match the values indicated by the initial test results before damage was inflicted. In each case of damage and repair, frequencies followed the expected pattern of frequency changes. That is, increased stiffness caused increased frequency. The finite element model followed the measured frequencies for each damage case. Experimental measurements tended to align lower than those estimated by the finite element model. Damage was shown to change the natural frequency of the bridge.

The last case study focused on the effect of boundary conditions on a bridge. Forced vibration and a live load test were implemented on a bridge for multiple damage conditions. The conditions tested were the initial state, with severed supports, and with the support restraint as reduced as possible. The final condition involved lifting the bridge and replacing supports with greased Teflon pads. Twenty five velocity transducers and 136 strain gauges were placed on the bridge to measure the response. Dynamic excitation occurred in both directions, and the live load test occurred for the last damage case. The first five modes were detected. Each mode showed a decrease in frequency from damage. The live load tests had their measured strains compared to a finite element model to check their accuracy. Changing the boundary condition had minimal effect on the measured strain from both tests and the finite element model. This test indicates the value of frequency monitoring in detecting boundary condition changes.

The case studies described indicate examples of structural monitoring being useful in field conditions of actual structures.

Temperature Effects on Frequency

Foust (2014) did a study focusing on the relationship between temperature and modal parameters. By using statistical methods, damage can more easily be detected by distinguishing it from environmental factors. The Lambert Road Bridge in California had a monitoring system installed that included in-deck thermocouples, strain gauges, velocity transducers, and tiltmeters. Using information from the tiltmeter and thermocouples, a relationship between modal frequencies and deck temperature could be compared. The bridge systems monitor the bridge during normal use.

Time domain records of tiltmeter and strain gauge readings were analyzed by Fast Fourier Transform (FFT) to determine natural frequencies. Signal processing had to be done to distinguish the different frequencies and eliminate the noise in the readings. Multiple instruments' data was compared to determine the natural frequencies of the bridge. The values were also compared to an earlier study where similar natural frequencies were discerned. These frequencies were accepted as the natural modal frequencies of the bridge.

In order to better understand the relationship between temperature and frequency, the temperature was observed in depth. Multiple thermocouples were set in the deck of the bridge and throughout the webbing. The temperature gradient was compared throughout the bridge throughout the day. It was shown that the temperature on the deck fluctuated much more than that of the interior of the bridge. The interior of the bridge generally had the same temperature, while the deck temperature could be as much as 15 degrees Fahrenheit higher to 5 degrees lower

than the interior of the bridge. From these measurements, the gradual process of heating the entire bridge is shown. There is no information relating the bridge temperature to the ambient temperature.

In order to compare dynamic factors with temperature, the standard deviations of all measurements were found and compared. The changes in all other measurements match the change in temperature, indicating the temperature change drives the fluctuations throughout the bridge. Temperature change can cause internal resistance, as the temperature change is not uniform throughout the bridge. It was determined that natural frequency was only affected by changes in temperature and not by other factors. The peak frequency was shown to be between the peak deck temperature and the peak lower temperature. Statistical regression models were then made between the temperature and the measured frequencies. It was shown that there was a positive relationship between frequency and temperature.

In order to determine the connection between frequency and temperature, an average thermocouple and frequency reading were compared. The average bridge temperature hits a peak near a peak in the natural frequency. In this way, disparity between the actual temperature across the bridge is somewhat accounted for. The Kuppa method was used to find the average temperature, giving a weighted average of temperature across the bridge. The relation between temperature and frequency is assumed to be linear. Regression models were created based on this assumption.

The first two modal frequencies were detected by all of the sensors, while higher frequencies were not detected as often and had greater variation in the data. Due to this, only the confirmed 3.1 Hz and 4.2 Hz frequencies were used for the regression models. Regression models were made from both average temperatures and specific temperatures near the sensor.

The temperature was shown to cause a minimum variation of 20% from the minimum natural frequency. This study indicated the importance of understanding a structure's dynamic behavior under normal dynamic conditions. It also provides a field example of the changes to a structure from temperature changes, indicating a correlation specific for this bridge.

Detecting and Modeling Dynamic Properties

Morassi did a study detailing the creation of a finite element model to match the measured dynamic properties of a bridge in Italy (Morassi and Tonon 2008). The primary focus of the paper is calibrating a SAP2000 model to match the acceleration detected from a shaker test. The bridge in question is a three-span overpass, consisting of a large post tensioned slab as the primary structural support. Only the first six modes of vibration were identified for this study.

Prior to testing, a finite element model was created to determine mode shapes and locate the proper locations for sensor and shaker placement. Initially, all of the elements were modeled along the center of gravity of the bridge. Prestress forces were ignored in this model, being shown to have little effect on the dynamic properties reported (Hamed and Frostig 2006). This model produced the expected mode shapes and allowed the proper placement of 10 accelerometers across the bridge.

Frequency response functions were determined for the measured data and compared to the data provided by the finite element model. Six mode shapes were detected experimentally, aligning with the first eight modes defined by the model. The first three modes were used to calibrate the model. Both the first and third modes were higher than those predicted by the

model, while the second mode was lower than that predicted by the model. A MAC analysis indicated a correspondence of over 95% for modes one and three, with a 75% correspondence of the second mode. An additional two modes generated by the model were not detected in the test because they were poorly excited during the shaker test.

Calibration of the model involved a more accurate shape design, mirroring the structure and including additional objects such as the sidewalk in the analysis. Two shell objects were used to more accurately define the structure. One shell represented the structural system, and the other represented the span of the deck. This decreased the MAC variance in the bending modes of one and three, but other modes had a greater variance. The designers then adjusted parameters individually, following an iteration method to further calibrate the structure. This included refining assumed boundary conditions and adjusting Young's Modulus in different sections across the bridge. The maximum adjustment for Young's Modulus was taken as 30%, and in some locations on the structure the full 30% adjustment was required. The adjusted stiffness indicated additional stiffness applied to areas most affecting modes 1 and 3 and a reduction in those areas affecting mode 2. This updated model adjusted the MAC analysis values to above 94% for the first three modes of vibration. The additional modes also had relatively high correspondence, from 60-80%.

The article indicates the importance of being able to calibrate a finite element model to match the current conditions and how an accurate model can reflect the behavior of the bridge in dynamic conditions. Also, additional studies can relate to the adjusted model knowing it accurately affects the behavior of the bridge.

Literature Review Summary

Structural health monitoring has the potential to elongate the service life of structures by detecting internal damage and prescribing a method to repair said damage. While damage to a system has been detected using dynamic properties, these methods have yet to find widespread use in the field. The literature describes efforts to move these principals from the lab into practice. Environmental effects, particularly temperature, have been determined to play a large role in the dynamic characteristics of structures. The literature indicates that damage detection is on a case by case basis and requires monitoring of the structure before damage occurs. By creating a baseline case for a structure, future changes can be monitored and detected. Those that deviate from the expected values could represent damage and require further investigation. By creating a group of baseline frequencies and mode shapes for the Nibley Bridge, changes throughout its life can be more easily detected and explained.

Chapter 2: Nibley Bridge Description and Instrumentation

Bridge Description

The Nibley Bridge is a recently constructed short bridge over the Blacksmith Fork River, connecting Highway 165 to the newly constructed high school in Millville. The bridge consists of ten girders 27.3 m (89.5 ft) long. The Nibley Bridge was planned with instrumentation before construction began. Sensors to measure strain, temperature, and acceleration are embedded in the bridge. Construction began in the fall of 2015, with the girders being cast in December. The bridge was opened to the public in August of 2016. Two girders were instrumented, one located on the outer edge of the bridge and the other located at the center of the bridge. Figure 2.1 shows a side image of the bridge.

Figure 2.1: Elevation View Looking North

Ten prestressed precast deck bulb T girders span the river and form the deck of the Nibley Bridge. Figure 2.2 shows the girders just after placement on the bridge. Each girder is 1.07 m (3.5 ft) high and has a 1.82 m (5.98 ft) flange width. The girders are spaced 1.83 m (6 ft)

on center. The upper flanges of the girders are grouted together, forming the deck of the bridge. Metal weld ties connecting the girders are spaced 305 mm (1 ft) from the end and 1.52 m (5 ft) on center across the bridge. The keyways are grouted with 58.6 MPa (8.5 ksi) strength grout along their length. The total girder span length is 27.28 m (89.5 ft), but the deck length spans only 25.91 m (85 ft).

The deck width is 18.29 m (60 ft) across. Two steel intermediate diaphragms connect the girders at third points of the span, as shown in Figure 2.3. These diaphragms stop for the steel sewer pipe that passes between girders 3 and 4. Both of these are indicated on Figure 2.4. Prestressed tendons were placed in both harped and straight patterns within the girder. The depth of the girder deck changes longitudinally across the bridge to keep the road flat. Decks are deepest on the ends to account for prestressing camber. They also slope laterally to provide a roadway cross slope. Eight piles support each abutment. After casting the abutment, girders were placed on bearing pads and the approach slab was cast around the girders. A parapet wall and sidewalk were cast on the exterior girders, extending 2.74 m (9 ft) from the side. A 76.2 mm (3 in.) asphalt layer covers the bridge deck.

Figure 2.2: Girder Placement during Construction (Ira Tibbits, personal communication, Oct. 18, 2016)

Figure 2.3: Diaphragm Connecting Girders of the Bridge

Figure 2.4 through Figure 2.7 define the bridge dimensions. Figure 2.4 shows a plan view of the bridge, with multiple section cuts called out. Figure 2.5 indicates the alignment of the girder, abutments, and parapet. Figure 2.6 indicates a half cross section of the bridge. Figure 2.7 indicates the dimensions for a typical girder.

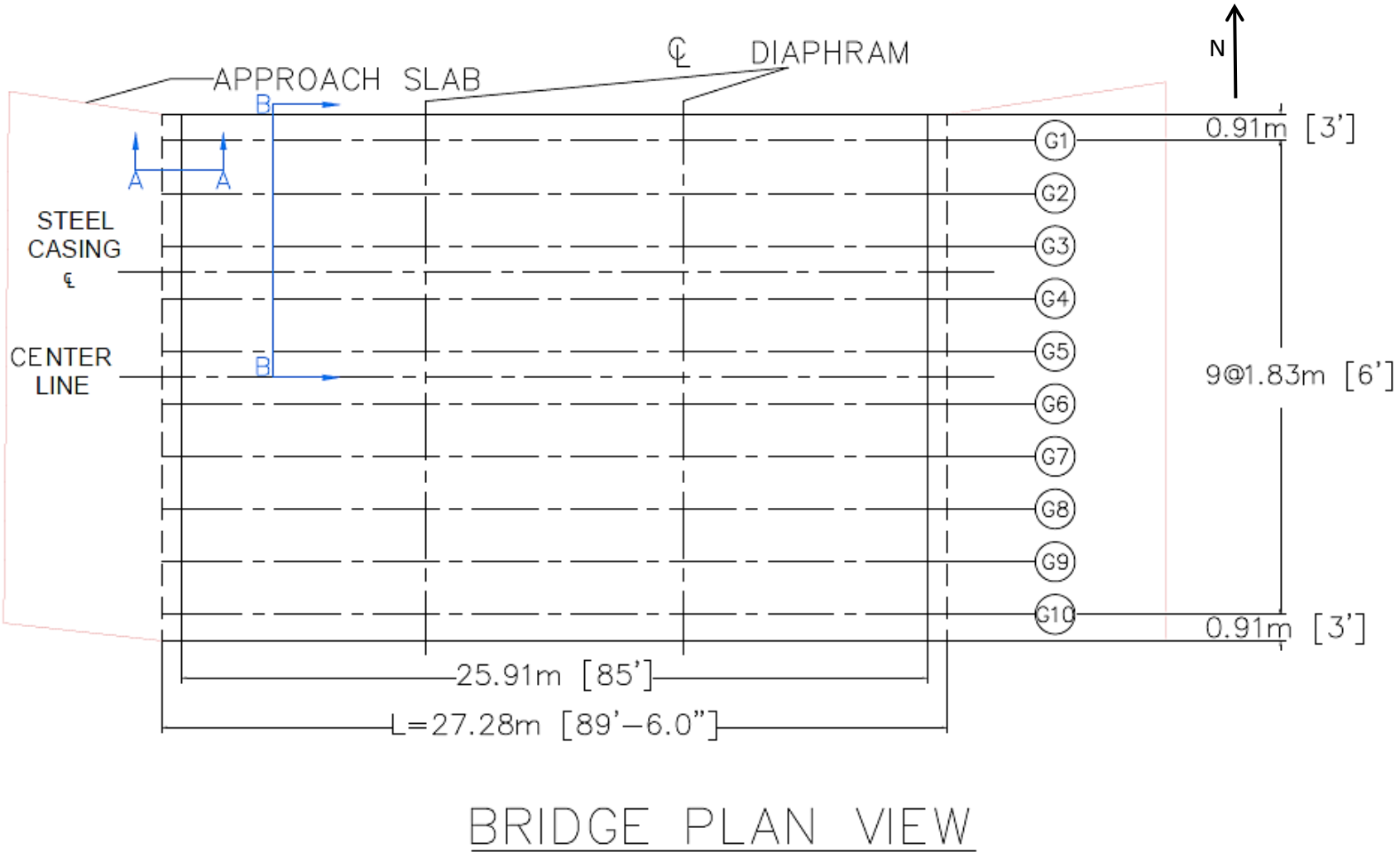

Figure 2.4: Plan View of the Nibley Bridge; Variable L is Defined in this Figure and will be used Elsewhere in this Document

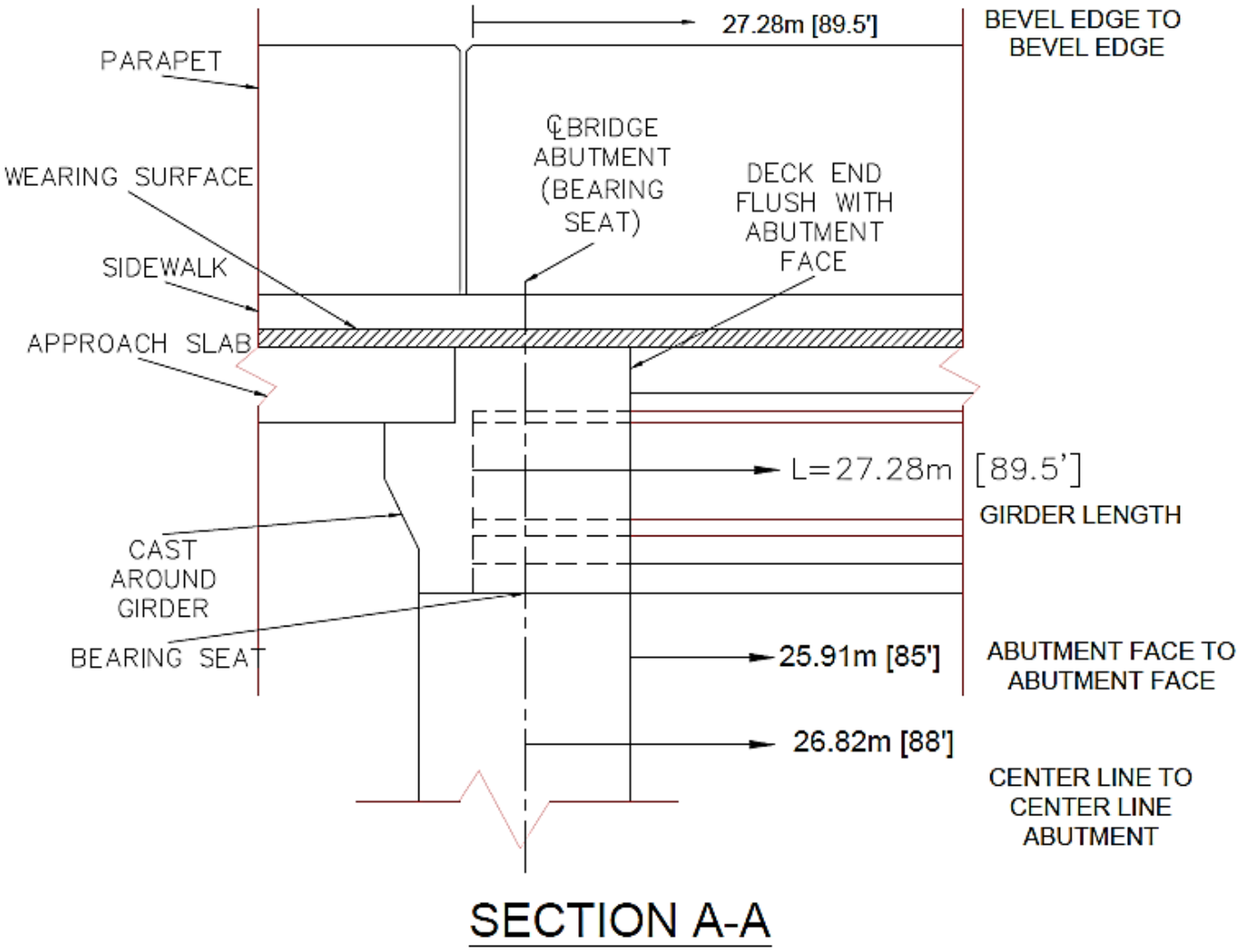

Figure 2.5: End Section of the Bridge, Section AA from Figure 2.4

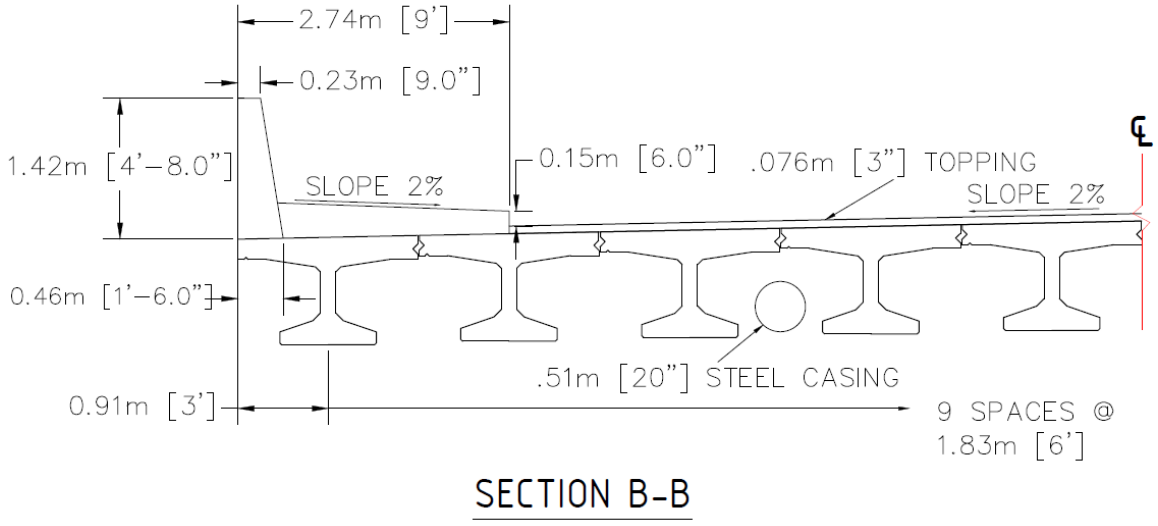

Figure 2.6: Half of Bridge Cross Section, Section BB from Figure 2.4

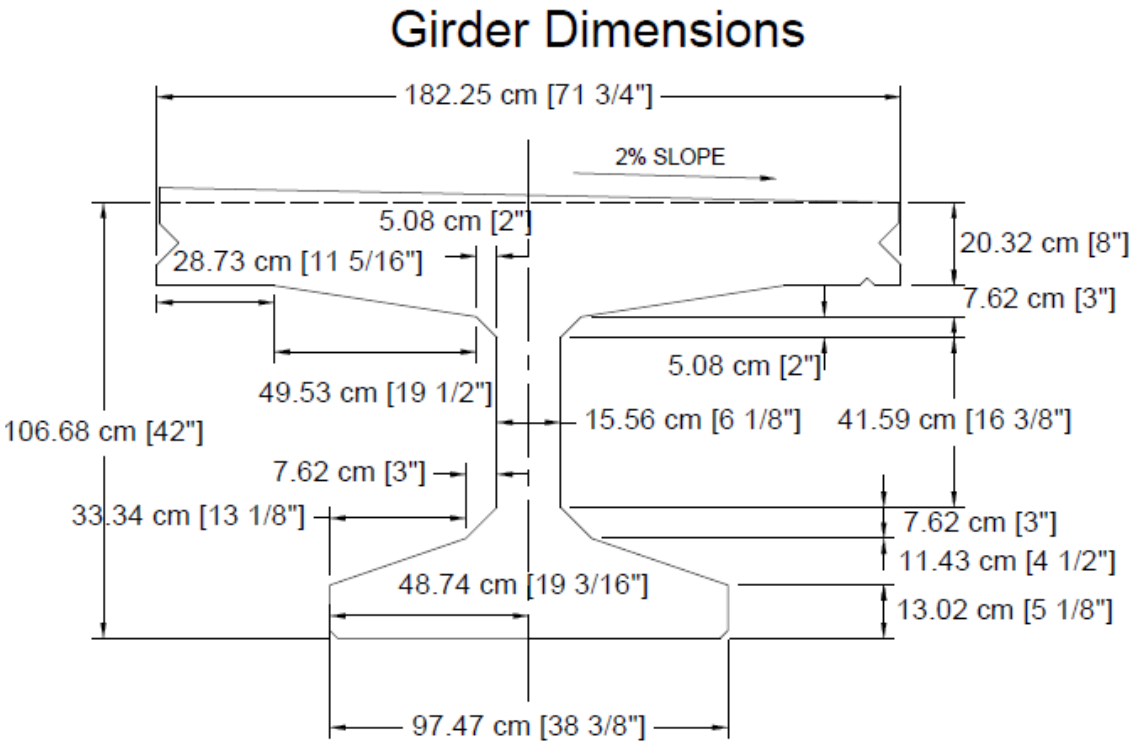

Figure 2.7: Construction Dimensions of a Typical Girder (Ethan Pickett, personal communication, Feb. 21, 2017)

Embedded Sensors

Embedded sensors were placed in five locations across two different girders in the bridge. Girder 1 and girder 5 are both instrumented. Strain gauges, thermocouples, and accelerometers are all embedded in these girders. The strain gauges and thermocouples were grouped together in clusters, which are labeled alphabetically. Accelerometers are labeled according to their location within the girder.

Figure 2.8 shows the sensor locations in plan view. To further illustrate the locations of the sensors, girder 1 and girder 5 are viewed in more detail in Figure 2.9. Girder cross sections are shown in Figure 2.10 through Figure 2.12.

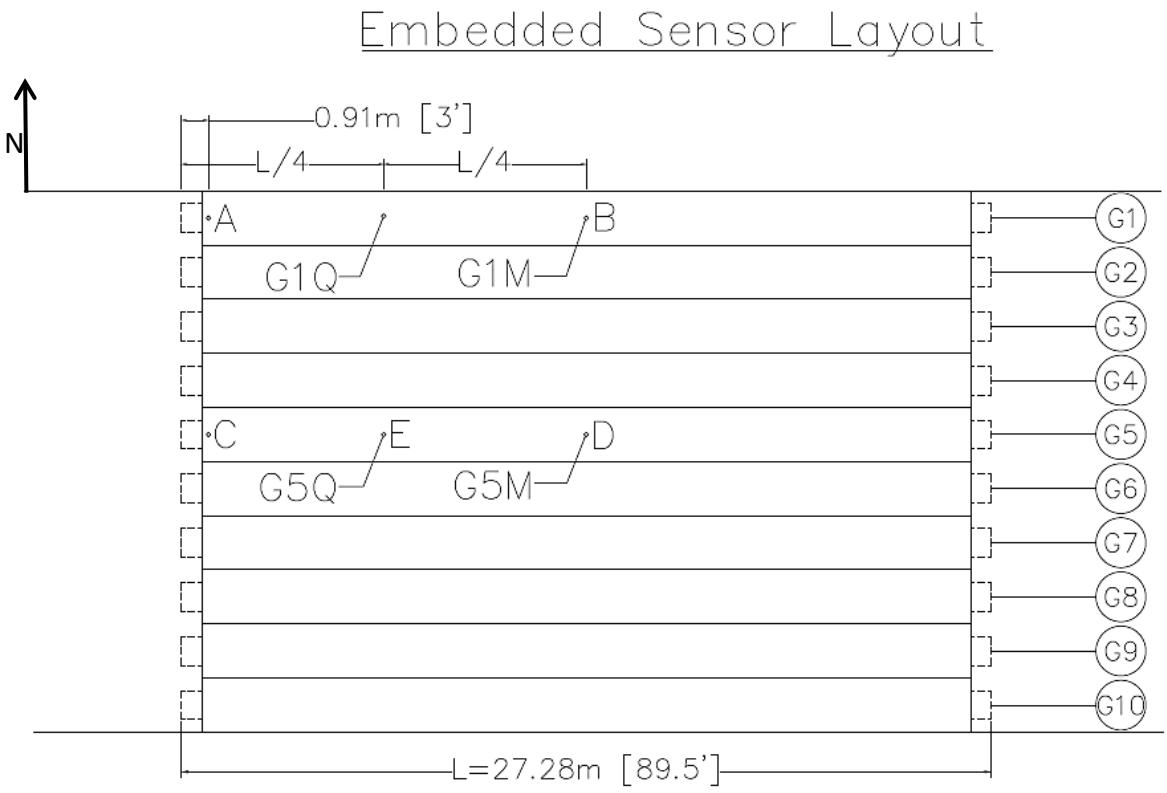

Figure 2.8: Instrument Layout Plan View

Figure 2.10 through Figure 2.12 indicate the depth and labeling of each sensor. Each sensor and their layout are described further in the following sections. Table 2.1 through Table 2.3 defines each sensor, location, and name for a quick reference guide. Though the strain gauges were not used for this study, they are mentioned for completeness.

Geokon strain gauges were placed on both sides of the bottom flange of the beam, and two are aligned vertically in the web. Each gauge measures longitudinal strain. The strain gauges are primarily for a different experiment regarding strain in the concrete occurring over the life of the structure. Figure 2.13 shows a strain gauge in place. Two sets of strain gauges are placed in each girder, one four feet from the end and one in the center of the girder. This pattern is repeated in both girders. They were labeled according to their sensor location within the sensor cluster.

Thermocouple bundles consisted of ten measurement locations spaced to cover a depth of 171.45 mm (6.75 in.). Depths were segmentally spaced, depths being at 0 mm, 6.35 mm (.25 in.), 12.7 mm (.5 in.), 19.05 mm (.75 in.), 31.75 mm (1.25 in.), 44.45 mm (1.75 in.), 69.85 mm (2.75 in.), 95.25 mm (3.75 in.), 133.35 mm (5.25 in.), and 171.45 mm (6.75 in.). Thermocouple wires were placed within a PVC pipe to maintain depth during casting and to protect the wire. One was placed with each strain gauge bundle, with the top sensor being in contact with the bridge deck. Girder 5 also included two smaller thermocouples, containing only the upper five sensors each. These thermocouples were placed in the top and bottom of the girder at quarter span. The thermocouples allowed the creation of a temperature gradient profile from within the center of the girder. Figure 2.14 shows a thermocouple placed before the girders were cast.

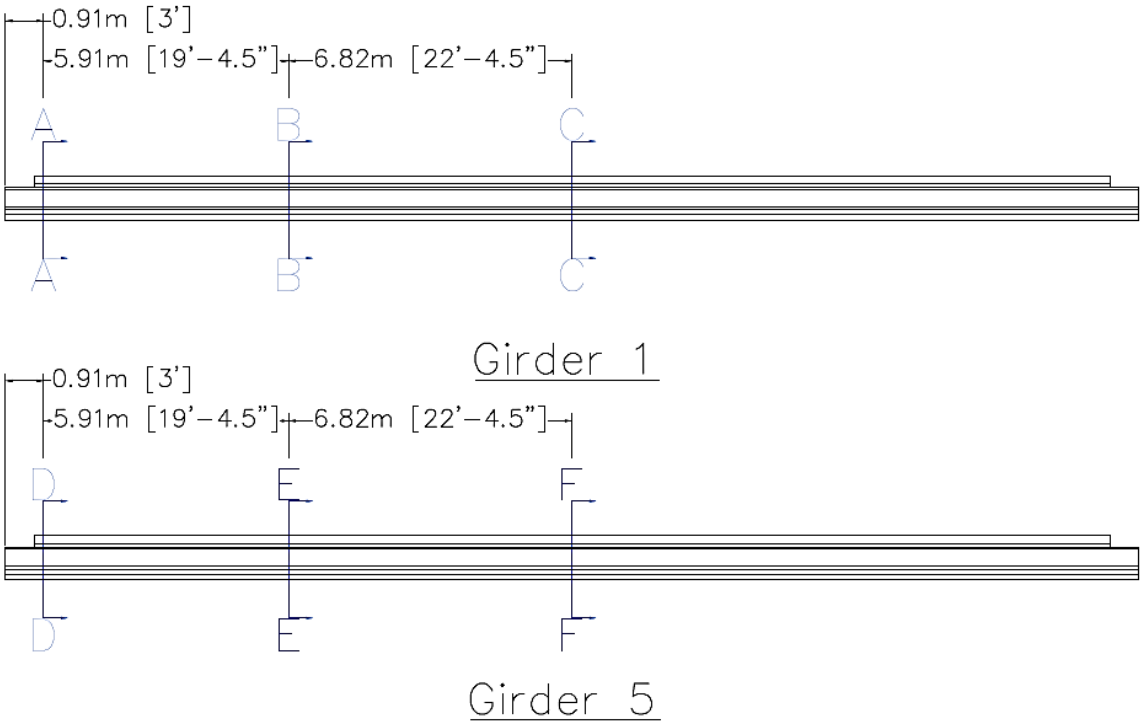

Figure 2.9: Girder 1 and Girder 5 Section Cut Locations

Table 2.1: Sensors Located in Section A-A and B-B

Table of Sensors			
Section Cut Location	Sensor Type	Name	Description
A-A	Thermocouple	A1	Sensor at depth 0 mm
		A2	Sensor at depth 6.35 mm
		A3	Sensor at depth 12.7 mm
		A4	Sensor at depth 19.05 mm
		A5	Sensor at depth 31.75 mm
		A6	Sensor at depth 44.45 mm
		A7	Sensor at depth 69.85 mm
		A8	Sensor at depth 95.25 mm
		A9	Sensor at depth 133.35 mm
		A10	Sensor at depth 171.45 mm
	Strain Gauge	AUW	Upper web gauge
		ALW	Lower web gauge
		ABR	Right bottom flange gauge
		ABL	Left bottom flange gauge
B-B	Accelerometer	G1Q	Girder 1 quarter span

Table 2.2: Sensors Located in Section C-C to E-E

Table of Sensors			
Section Cut Location	Sensor Type	Name	Description
C-C	Thermocouple	B1	Sensor at depth 0 mm
		B2	Sensor at depth 6.35 mm
		B3	Sensor at depth 12.7 mm
		B4	Sensor at depth 19.05 mm
		B5	Sensor at depth 31.75 mm
		B6	Sensor at depth 44.45 mm
		B7	Sensor at depth 69.85 mm
		B8	Sensor at depth 95.25 mm
		B9	Sensor at depth 133.35 mm
		B10	Sensor at depth 171.45 mm
	Strain Gauge	BUW	Upper web gauge
		BLW	Lower web gauge
		BBR	Right bottom flange gauge
		BBL	Left bottom flange gauge
	Accelerometer	G1M	Girder 1 mid span
D-D	Thermocouple	C1	Sensor at depth 0 mm
		C2	Sensor at depth 6.35 mm
		C3	Sensor at depth 12.7 mm
		C4	Sensor at depth 19.05 mm
		C5	Sensor at depth 31.75 mm
		C6	Sensor at depth 44.45 mm
		C7	Sensor at depth 69.85 mm
		C8	Sensor at depth 95.25 mm
		C9	Sensor at depth 133.35 mm
		C10	Sensor at depth 171.45 mm
	Strain Gauge	CUW	Upper web gauge
		CLW	Lower web gauge
		CBR	Right bottom flange gauge
		CBL	Left bottom flange gauge
E-E	Thermocouple	E1	Sensor at depth 0 mm
		E2	Sensor at depth 6.35 mm
		E3	Sensor at depth 12.7 mm
		E4	Sensor at depth 19.05 mm
		E5	Sensor at depth 31.75 mm
		E6	Sensor at 0 mm from bottom
		E7	Sensor at 6.35 mm from bottom
		E8	Sensor at 12.7 mm from bottom
		E9	Sensor at 19.05 mm from bottom
		E10	Sensor at 31.75 mm from bottom
	Accelerometer	G5Q	Girder 5 quarter span

Table 2.3: Sensors Located in Section F-F

Table of Sensors			
Section Cut Location	Sensor Type	Name	Description
F-F	Thermocouple	D1	Sensor at depth 0 mm
		D2	Sensor at depth 6.35 mm
		D3	Sensor at depth 12.7 mm
		D4	Sensor at depth 19.05 mm
		D5	Sensor at depth 31.75 mm
		D6	Sensor at depth 44.45 mm
		D7	Sensor at depth 69.85 mm
		D8	Sensor at depth 95.25 mm
		D9	Sensor at depth 133.35 mm
		D10	Sensor at depth 171.45 mm
	Strain Gauge	DUW	Upper web gauge
		DLW	Lower web gauge
		DBR	Right bottom flange gauge
		DBL	Left bottom flange gauge
	Accelerometer	G5M	Girder 1 mid span

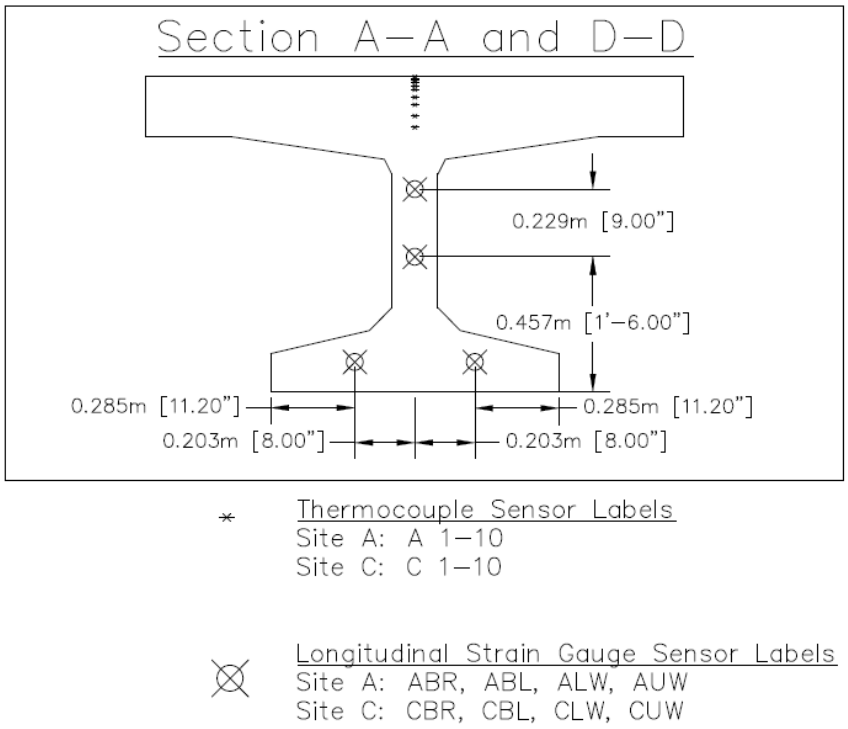

Figure 2.10: Instrument Layout, Sections A-A and D-D

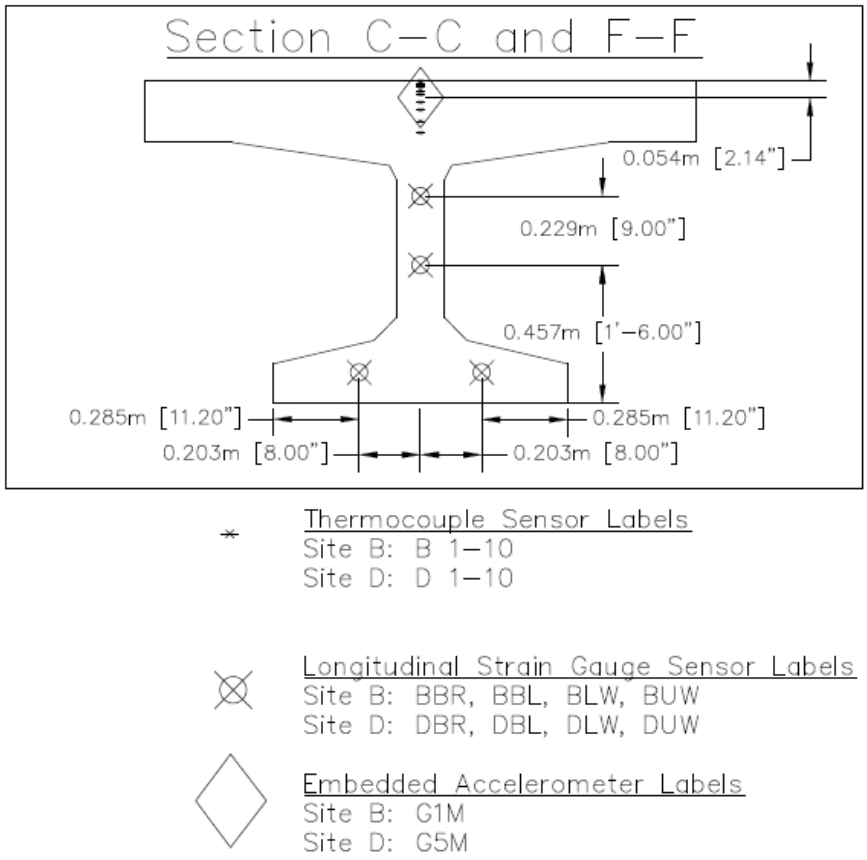

Figure 2.11: Instrument Layout, Sections C-C and F-F

Measurement Specialties triaxial accelerometers were selected for this project based on availability. The accelerometers are embedded within the bridge at midspan, 13.49 m (44.25 ft), and quarter span, 6.74 m (22.12 ft). Accelerometers were mounted to a metal brace to maintain axial alignment during casting. Silicone and bubble wrap were used to waterproof and protect the sensors as shown in Figure 2.15. These locations were chosen to maximize detection of the first three vertical modes.

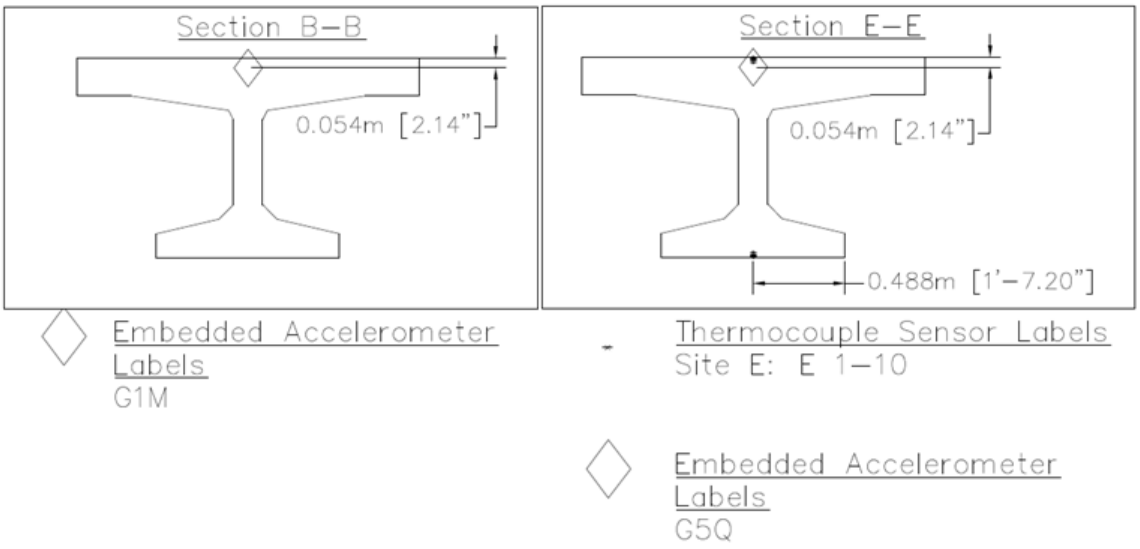

Figure 2.12: Instrument Layout Section B-B and E-E

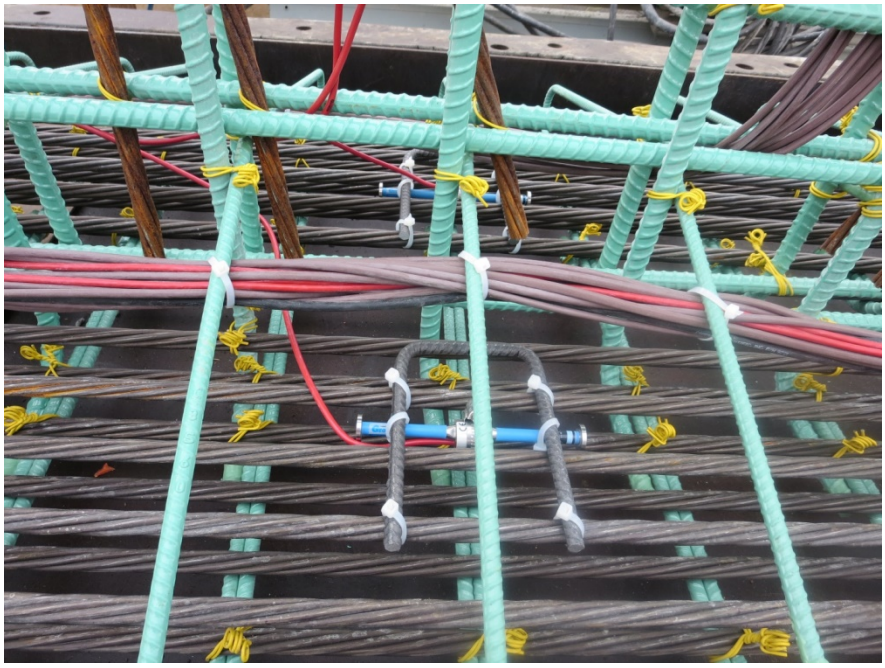

Figure 2.13: Strain Gauge placed in the Web

Figure 2.14: Thermocouple Placement during Construction

Additional Sensors and Excitation System

Additional sensors were used to calibrate the embedded sensors and to define the modal characteristics of the bridge. Multiple tests were performed using L-4C Geophone velocity transducers to obtain data. Three tests were done over the course of many months in the fall of 2016. An impact test was performed prior to asphalt being placed on the bridge on June 29th. A vertical shaker test was performed on August 12th after the asphalt was placed. A second shaker test was performed on October 20th. The goal of this test was to confirm and expand the dynamic results of the first shaker test. For the first two tests, data from the embedded sensors were recorded for comparison.

The velocity transducers were placed on the surface of the bridge and measured velocity in the vertical direction. Figure 2.16 shows a velocity transducer on the bridge during the impact test. Sensor locations were selected to calibrate the embedded sensors and detect the natural

frequencies of the bridge. For this reason, sensors were placed near the embedded sensors and along the bridge.

Figure 2.15: Embedded Accelerometers during Construction

An APS Dynamics shaker was used to excite the bridge, shown in Figure 2.17. The shaker provided excitation in the vertical direction. This shaker has been retrofitted to allow easy placement and transport. The shaker itself weighs 73 kg (160 lb.) and provides excitation at a peak force of 445 N (100 lb.). The intensity of the excitation was not recorded as part of this project.

Data Acquisition System

Embedded sensors have been monitored periodically from casting up to the current day. Because utilities have still not been completely installed on the bridge, the accelerometers were not typically measured and have only been read on short term occasions. Dataloggers were provided by Campbell Scientific. Multiple dataloggers have been used to read the accelerometers throughout their lifespan, including the CR1000, CR3000, CR9000, and CR6. These systems are useful in their robustness and low power cost but have difficulty collecting the large data measurements required for dynamic processing. Strain gauges and thermocouples

have been monitored frequently, while the accelerometers proved more difficult to collect meaningful data.

Figure 2.16: Velocity Transducer on the Bridge prior to Asphalt Installation

Figure 2.17: APS Shaker during First Shaker Test

There were two main difficulties in obtaining dynamic measurements. The first is an issue known as digitization. Digitization occurs when the datalogger converts the analog signal it receives into numerical data. The digital, or numerical, data has a limited amount of values it can be, based on the number of bits the datalogger has. When an analog signal is between two of the possible digital values, the datalogger will round the value to one of these digital values and store that information. This can be referred to as the precision of the datalogger. Typically, precision isn't a problem because variances in sensor readings are much larger than the possible values allowed by digitization. In the case of the Nibley Bridge, poor precision and low excitation made collecting data difficult. Campbell Scientific dataloggers typically have a 12 bit precision, which limits how precise the measurements can be. By using different dataloggers, the effects of digitization were able to be mitigated to a point. Further examples of this concept and the effectiveness of the embedded sensors are discussed later.

A Data Physics Savant model was used to record readings from the velocity transducers. This system was able to sample at a high frequency and had 24 bit precision. The Data Physics system was only in use during the three tests that were performed on the bridge.

Chapter 3: Test Methods and Goals

This chapter describes the methods used to determine the dynamic characteristics of the bridge. Multiple tests and sensor layouts were used as part of the study on this bridge. This chapter is divided into sections correlating with each test, describing the goals and methods for each case. Ultimately, the dynamic properties of the bridge were ascertained primarily by the three short term tests, but the long term monitoring system is described here for completeness.

Long Term Monitoring System

The embedded sensors were installed to monitor the bridge continually over the course of multiple years. The Nibley Bridge was designed with monitoring being a primary goal. Long term monitoring requires adequate power supply and data storage. For the dynamic system to be fully monitored, the site would need to have power and an internet connection to upload the collected data. Throughout the course of this study, construction of utilities around the bridge was incomplete. For this reason, long term monitoring is not included as part of this study. Data from the embedded accelerometers has been collected periodically over their lifetime.

Monitoring of the embedded sensors occurred multiple times, but primarily only three of these times provided useful data. Two of those times were during the tests described in the following sections. Additionally, the embedded sensors were monitored while the girders were in transit from the casting yard to the construction site. Monitoring during transit was done by a CR6 sampling at 200 Hz. This data isn't used for this study. The data collected does indicate that the CR6 can be used for monitoring of the accelerometers. A large goal of this paper is to ascertain the usefulness of the embedded sensors and the data collection system. As part of the

long term monitoring system, it is important that the appropriate datalogger be used. The CR6 functioned well enough to be considered a reliable datalogger.

The long term monitoring system was planned to function on an intermittent schedule. The primary goal of long term monitoring was to correlate natural frequency and temperature. Because the bridge temperature changes very slowly, measurements once every hour are typically sufficient. The accelerometers would be active a few minutes of every hour to detect frequencies. A comparison between frequency and bridge temperature could then be ascertained. A CR1000 was in use by the other sensors at the site and was initially used for the dynamic monitoring as well. Data collected by the CR1000 tended to be blocky, suffering from digitization. Digitization occurs as the datalogger converts an analog signal into numerical digits. This is also described as the precision of the datalogger. Typically, the measured amplitude is much larger than the precision, so the precision is barely noticeable. However, in this case, acceleration was only a few times larger than the precision of the CR1000, resulting in data that contained only a few different numerical points. A CR3000 was then used due to it having a higher precision than the CR1000, but the data was still too digitized to detect frequencies during only ambient excitation. The data collected over this period was unusable for determining the natural frequency of the bridge. Both dataloggers sampled at 100 Hz, and the sampling was done before the bridge was open to traffic.

In order to troubleshoot the embedded sensors, it was decided to use an additional monitoring system to calibrate the embedded accelerometers. Multiple tests were run to not only test the effectiveness of the embedded sensors but to establish the modal parameters of the bridge as well.

Impact Test

There were two main goals of the impact test. The first was to test the sensitivity of the embedded sensors against the external sensors. The second goal was to determine the natural frequency of the bridge prior to asphalt installation. To correlate the embedded sensors, the velocity transducers and data physics system were used. The test involved seven velocity transducers and the four embedded accelerometers. A picture of the test is shown in Figure 3.1.

The sensors were placed to compare the response between the velocity transducers and the accelerometers. Excitation was caused by dropping a pick axe, shown in Figure 3.2. Multiple hits were performed at each location. Excitement locations were near the embedded accelerometers to maximize their response to the test. Along with the impacts, ambient excitation from walking on the bridge also occurred.

Figure 3.1: Preparing Sensors for the Impact Test

Figure 3.2: Pickaxe used to Excite the Bridge during Impact Test

The embedded accelerometers were monitored by a CR3000 datalogger sampling at 100 Hz. Only the vertical direction was sampled. The velocity transducers were sampled at 512 Hz. Sensor layout and impact locations are shown in Figure 3.3.

Prior to this test, it was unknown if the accelerometers were recording the proper amplitude or if they were damaged during the casting process. By differentiating the velocity transducers, the acceleration of the two types of sensors could be compared. In this way the recorded response of the accelerometers could be validated.

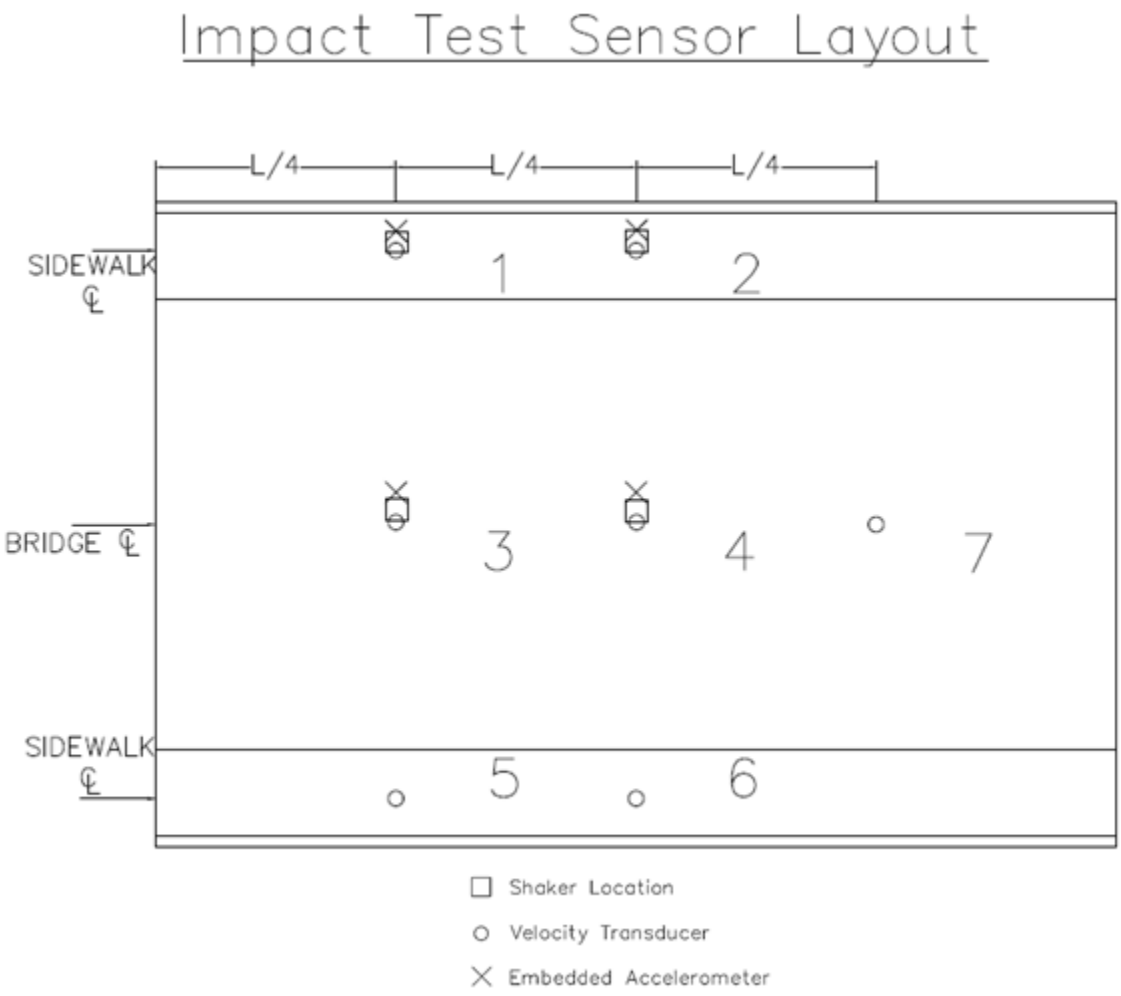

Figure 3.3: Sensor Layout during the Impact Test

Using MATLAB's "diff" function, the recorded velocity was converted to an acceleration to be compared. The diff function returns the difference between consecutive points of the input vector. After converting both responses to units of m/s^2, the time histories were aligned to compare the response for each impact point. The time history of a function is the response detected by a sensor. An example of ambient excitation taken from the second shaker test is shown in Figure 3.4. In the example, crossing vehicles are represented by the large amplitude spikes shown. The time history can be used to determine the modal characteristics and frequency response of the bridge, not just the acceleration at any time.

Frequency response of the bridge was determined using the data physics system. The data physics system automatically returns the auto power spectrum of the recorded data. The method is similar to the one described below, which is applied to time histories in MATLAB. The power spectrum returned for the time history above is shown in Figure 3.5. As mentioned, the accelerometer data was too digitized to allow for an accurate power spectrum to be determined. Results of these methods are described in Chapter 4.

The auto power spectrum shown shows the distribution of the energy contained in the time history. Peaks in the power spectrum represent a larger portion of the energy occurring at the indicated frequency. By selecting the peaks, the natural frequencies of the structure can be gleamed. As indicated in Figure 3.4, the entire signal is fairly noisy. This is due in part to the excitation being from ambient sources. Windowing and other processing methods can flatten the data, but are able to provide more accurate results.

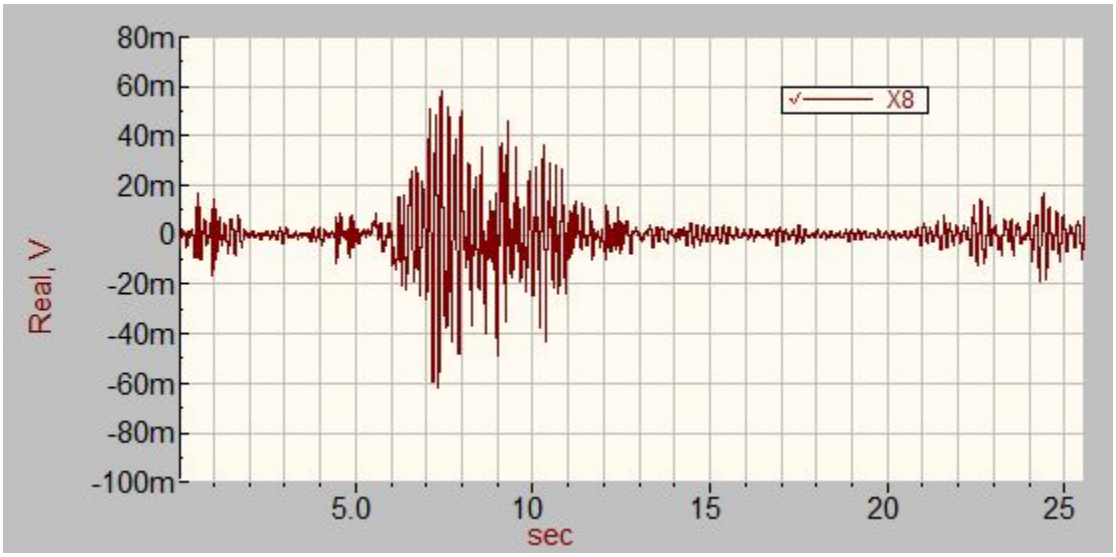

Figure 3.4: Time History of Ambient Excitation of a Velocity Transducer

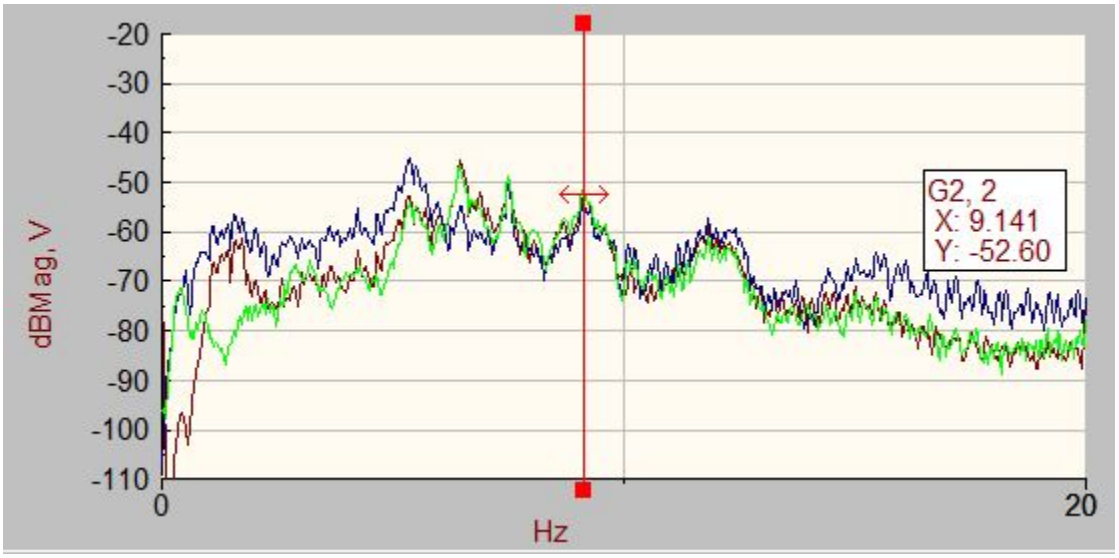

Figure 3.5: Plot of the Auto Power Spectrum of Three Sensors

Frequency response of the embedded sensors was also considered. Using MATLAB's "pwelch" function, the power spectrum reported by the accelerometers could be determined. The pwelch function uses Welch's overlapped segment averaging to estimate the power spectrum density (Mathworks 2016). Welch's method uses multiple overlapping segments of the original data (Welch 1967). After overlapping, the segments are windowed by a Hamming window. Overlapping of the data also serves to mitigate the unbalanced shift created by the window. A periodogram is then calculated by computing the Discrete Fourier Transform (DFT) and squaring the results. The resulting periodograms are then averaged, resulting in a power spectrum with reduced variance.

Windowing is a method to reduce the detected spectral densities to those contained within the time history. A Hamming window reduces the values of the time histories to zero at the edges of the windowed segment, thus removing those periodic values that extend beyond the range of the time history. This improves the values returned by the DFT and helps to eliminate false results due to the finite length of the time history (Smith 2011).

The Fourier transform determines the components of a time-based signal. The Fourier series expands a periodic function into a summation of sine and cosine values. The Fourier transform generalizes the Fourier series infinitely, changing the sum to an integral. The resulting function represents the decomposed time signal (Weisstein 2017). Using a method from signal processing called the Fast Fourier Transform (FFT), a signal can be converted into a power spectrum. Applying the transform to the windowed time history returns the power spectrum, which was described above.

Signal processing methods are integral in determining the change in natural frequency that occurs due to changes to the structure. Comparing the dynamic state of the bridge during each of the tests provides insights into the changes that have occurred. Comparing the frequency response of the bridge is a key aspect of setting up a long term monitoring system for the structure.

First Shaker Test

The first shaker test had multiple goals. As with the impact test, calibration of the embedded accelerometers was a main goal. Additional goals were to confirm the natural frequencies detected during the impact test and to detect the frequency change due to the added asphalt. Lastly, by using the shaker, the steady state condition could be used to detect the mode shapes of the bridge. Figure 3.6 shows the first location of the shaker during the test.

A CR9000 was used to sample the embedded accelerometers. This system boasts a much faster sample rate than other Campbell Scientific dataloggers, as well as improved resolution to mitigate the effects of digitization. The CR9000 sampled at 5000 Hz during the test. Using this system, the noise in the embedded sensor signal could be easily determined. The difficulty with

the embedded sensors included a large amount of sensor noise. Although some noise is expected, the noise ratio of the embedded sensors proved to be significant. Because the problems arising from data collection, namely digitization and a low sample rate, were mitigated during the test, issues with the sensors themselves became more apparent. By analyzing this data, recommendations for the future use of the embedded sensors could be determined.

Figure 3.6: First Shaker Test

The velocity transducers were sampled at 1280 Hz, using the data physics system. This sampling rate was determined to be sufficient for the applied excitation. Though the bridge was closed to the public, large construction vehicles occasionally crossed the bridge during the test. Eleven velocity transducers were spaced on the bridge, again aligning with the embedded sensors and in an effort to cover the mode shapes of the bridge. Though the sensor was responding, it was determined later that the data from sensor 7 was incorrect, and the response measured by

this sensor was ignored. Figure 3.7 shows a view of the sensors aligned on the north side of the bridge.

Figure 3.7: View along the North Side of the Bridge during the Test

Excitation occurred in two places on the bridge. The sensor layout and excitation locations are shown in Figure 3.8. To accommodate traffic, the south lane of the bridge was left open. Testing began with swept sine excitation ranging from 1 to 50 Hz. Further swept sine signal excitations were done narrowing the frequencies to below 20 Hz. The first five mode shapes were determined to be below this frequency. After detecting the first five modal frequencies using the auto power spectrum, each frequency was excited in turn to discern the modal characteristics evident in the time histories at steady state. Frequencies 0.1 Hz above and below the peak power spectrum frequencies were also excited. After the shaker was moved, the

swept sine test was repeated in the new location. Shaker intensity was not recorded, only the frequency it was shaken at. The intensity was changed at various times to sufficiently excite the embedded accelerometers. The increase in excitation was required to detect it above the noise of the system.

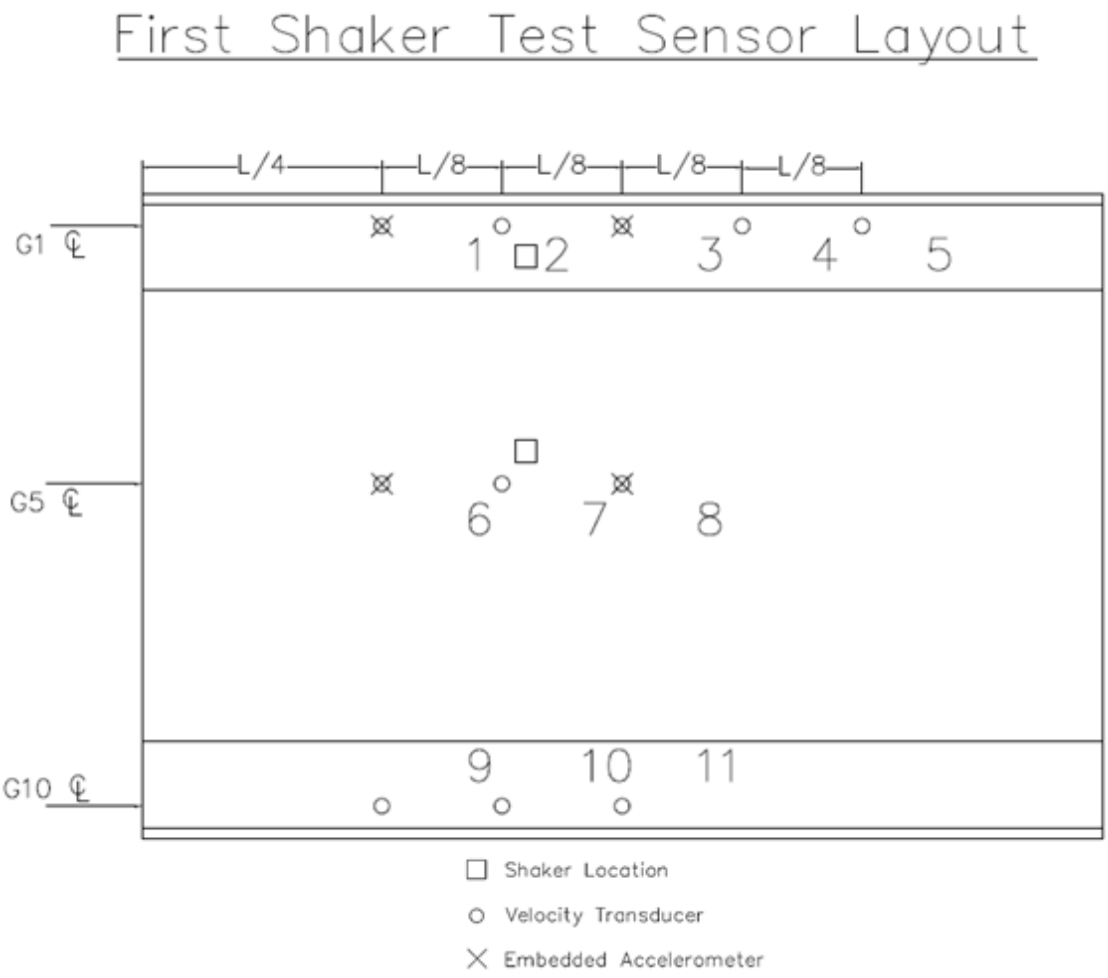

Figure 3.8: Sensor Layout during the First Shaker Test

Using the results of this test, natural frequencies and amplitudes detected by both monitoring systems could be compared, using the same methods as described in the Impact test. Mode shapes were determined by comparing the steady state response of the velocity transducers at various frequencies. Effort was made to align the time history as close to in phase or 180° out

of phase with each other. This method was also used to validate the indicated frequencies from the power spectrum.

Second Shaker Test

The second shaker test was planned to detect a change in the first five natural frequencies of the bridge due to the temperature difference between the first and second shaker tests. Additionally, a more accurate definition of the detected mode shapes was desired. The first shaker test indicated that vertical mode shapes were primarily differing laterally across the bridge. That is, the amplitude differences and nodes occurred in the lateral direction. The modes were measured only in the vertical direction. As shown in Figure 3.9, the layout of sensors was focused in the lateral direction rather than the longitudinal direction as in the layout of the first test. As with the first shaker test, the south lane was left open to allow for the flow of traffic. The bridge was open to the public at this time.

Only the velocity transducers were used in the second shaker test, using the aforementioned data physics system. Fifteen velocity transducers were spread across the bridge. These were sampled at 2560 Hz to increase the number of bins indicated by the power spectrum. Excitation occurred in two separate places, mirroring the first shaker test. The sensor and excitation layout is shown in Figure 3.9.

Similar to the first shaker test, excitation began with a swept sine signal ranging from 5 to 15 Hz. Detected frequencies were then excited in turn, with the effort being to determine the resonant frequency using the shaker and the time history. Traffic occurred during most of the shaker tests, as there was a fairly consistent flow of traffic. Gaps between traffic were long enough to establish a steady state response of the structure to continuous sinusoidal excitation.

Ambient response of the structure was also recorded. Because the embedded sensors have a large noise amplitude, knowing the amplitude generated by ambient response could help define how useful the embedded sensors would be. If the noise amplitude overpowered the ambient response, it is likely the embedded sensors would be useless. Data processing for this test was done in the same way as the first test. A picture of the sensors on the bridge is shown in Figure 3.10.

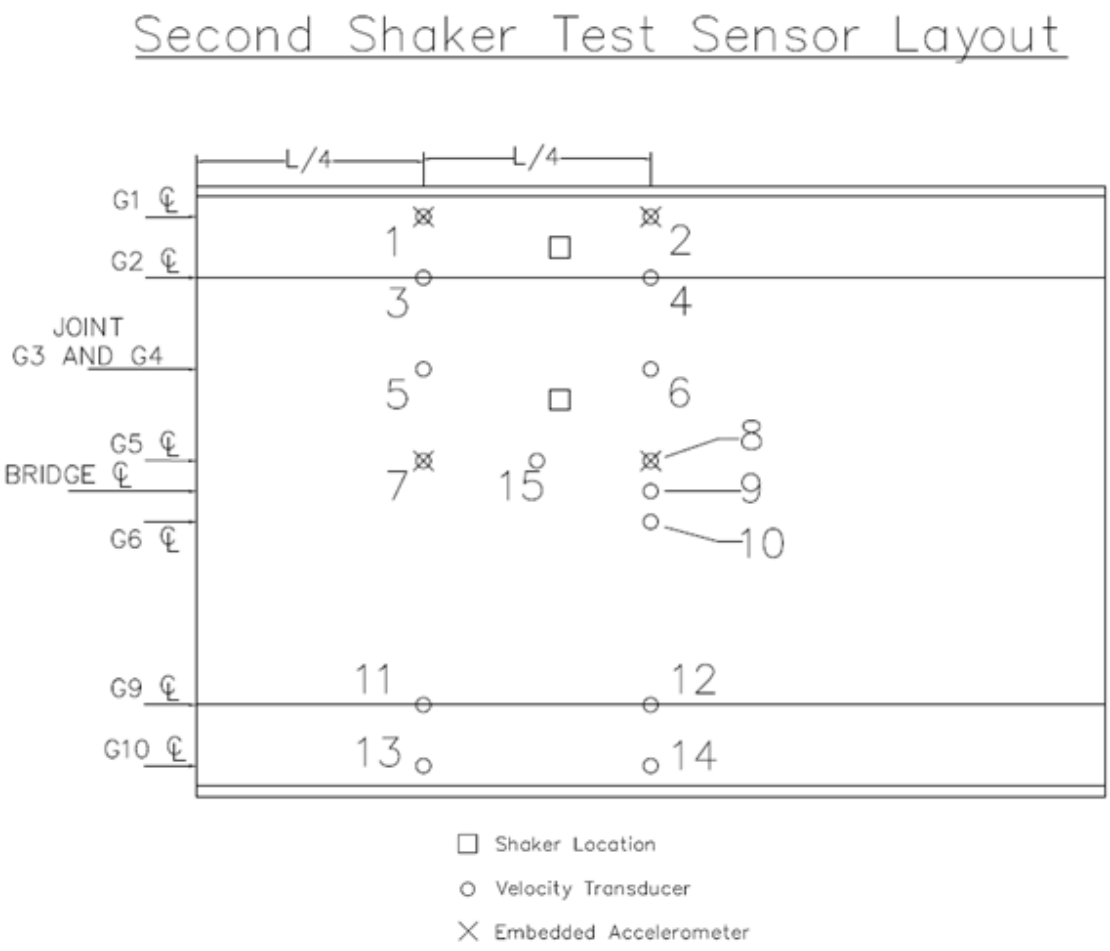

Figure 3.9: Sensor Layout during the Second Shaker Test

Finite Element Model and MAC Analysis

After the shaker tests, it was decided to create a SAP2000 model to evaluate the experimental modes against predicted modes of the finite element model (SAP2000 v. 18.0.1. 2015. Computers and Structures, Inc.). SAP2000 is a CSI finite element modeling program that can perform modal analysis using both Eigenvectors and Ritz vectors. The precast girders were modeled as elements, with the deck portion of the girder being modeled as shell elements. To compensate, the depth of the girder elements was modeled with a reduced deck. These elements were then connected with welds at the joints, linking the equations of motion for the deck and the corresponding girder. Prestressing forces in the concrete have a debatable effect on natural frequency. Hamed and Frostig (2006) indicated mathematically that forces caused by prestressing wouldn't change the dynamic properties of a structure. Other writers claim it can lower the measured frequencies. The experimental results recorded by Miyamoto indicated a slight decrease in measured frequencies when external prestressing forces were applied (Miyamoto et al. 2000). Including prestress forces in the SAP model did not show any change in mode shape or frequency. The prestress load effect was used as part of the analysis, but didn't appear to affect the results. The unmodeled prestressing effect may explain some error between the measured and analytical values but this error would likely be small. Model supports were modeled using stiff springs to reflect fixed behavior from the cast concrete. For the initial model, the stiffness of the supports was based on the typical values suggested by CSI, being 1E+11 kN-m/rad (8.51E+11 kip-in./rad) (Kalny 2014). Multiple initial models were made and compared to find a starting model, which found that these values were too stiff.

Figure 3.10: Sensors and the Shaker during the Second Shaker Test

Correlation between the model mode shapes and the measured mode shapes was performed using the Modal Assurance Criterion (MAC). A MAC analysis compares mode shapes for how similar they are, where a value of one indicates they are identical and a value of zero shows the modes have no correlation. This is due to the orthogonality property of modes. Chopra explains that the natural mode shapes satisfy the orthogonality properties (Chopra 2012). In terms of vector space, orthogonality exists when the dot product of two vectors is zero, indicating the vectors are at 90 degrees of each other. This same property exists for the natural frequencies of a structure, as demonstrated by Equation 1.

When $\omega_n \neq \omega_r$,

$$\Phi_n^T \boldsymbol{k} \Phi_r = 0 \qquad \Phi_n^T \boldsymbol{m} \Phi_r = 0 \qquad (1)$$

The above equation is based on the necessity of the system to align with the equation of free vibration, **m**

$$MAC := \frac{(\mathbf{x}_m^T \mathbf{x})^2}{(\mathbf{x}_m^T \mathbf{x}_m)(\mathbf{x}^T \mathbf{x})} \qquad (2)$$

$\mathbf{x}_{\boldsymbol{m}}$ is the measured mode shape vector

$\mathbf{x}$ is the analytical mode shape vector

It is important to note that this method does not verify the orthogonality of the modes. It only indicates that the modes are consistent. If errors exist, particularly in the case of invalid assumptions, consistent errors can be present in all modal vectors. Methods to correct this and other potential shortcomings of the method are related by Allenmang (2003).

Another source of error can be the analytical modes. SAP models can be solved in two ways, using Eigenvectors or using Ritz vectors. Eigenvectors are the traditional method to determine natural modes, and are created from the equations of motion referenced above. These vectors are very common and their derivation is explained by many authors such as Chopra (2012). In analyzing the recorded mode shapes, it was apparent that the response was relative to the force acting on the bridge. While Eigenvectors work well at reflecting the free vibration of a structure, Ritz vectors are able to account for the location of forcing. Both vectors were used in comparing the analytical model to the measured data, and both indicated identical results in the model.

An initial correlation indicated how well the predicted model matched the measured mode shapes. The values indicate what differences would be expected between a pre-made analytical model and reality, even only a few months after construction. This comparison, and the resulting correlation process, is carried out entirely in chapter four.

These values served as a starting point for further calibration of the model. Modal calibration can be difficult because many parameters affect modal properties, and knowing which to change can be difficult. Typically, manual updating based on engineering skills does not yield proper results. Iterative computational methods have been created to solve the modal problem and create an updated model that matches the measured structural response. Each method begins with the use of a residual, ε, the difference between the measured values and those reported by the analytical model. Residuals are defined by the modal characteristics, mainly the eigenvalues and eigenvectors of a system. The process of determining residuals and updating the analytical model are explained here. The methods described were taken from multiple papers, which will be referenced throughout.

The weighted least squares technique involves weighting the residual matrix. The equation is defined as:

$$\boldsymbol{\varepsilon}_W = \mathbf{W}_v\left(\mathbf{v}_M - \mathbf{v}(p_i)\right) \qquad (3)$$

$\mathbf{W}_v$ is the weighting matrix

$\mathbf{v}_M$ is the measured vector

$\mathbf{v}(p_i)$ is the analytically determined vector, a function of parameters p_i

($i=1,\ldots n_p$ =number of correction parameters)

Link (2001) presented the objective function described in Equation 3. The objective function is the weighted squared residual function. The minimization of this function represents a minimal difference between the measured and analytical values.

$$J = \varepsilon_W^T \varepsilon_W \quad (4)$$

Minimization of the objective function yields the unknown parameters. Along with the difficulty of multiple parameters, the results of the analysis vector are typically non-linear. Minimization thus requires the analytical vector to be expanded to a Taylor series, truncated at the linear term, or the point of interest.

$$\mathbf{v}(p) = \mathbf{v}_a + \mathbf{G}\Delta\mathbf{p} \quad (5)$$

$\mathbf{v}_a$ represents the analytical vector at linearization point $p = p_a$

$\mathbf{G}$ represents the sensitivity matrix of the system

$\Delta\mathbf{p}$ represents the unknown vector parameter changes

By linearizing the equation, parameters satisfying the objective function can be determined. These parameters then can be used to create a new analytical model, and the process can be repeated. Because the model isn't actually linear, multiple iterations are required before the values merge. To facilitate linearization, the creation of a sensitivity matrix is essential. The sensitivity matrix is defined in Equation 6 and indicates the partial change in the response vector due to the change in parameters at the linearization point.

$$\mathbf{G} = \frac{\partial \mathbf{v}}{\partial \mathbf{p}} \quad (6)$$

Inserting equation (5) into equation (3) yields the following linear residual equation:

$$\varepsilon_W = \mathbf{W}_\mathbf{v}(\mathbf{v}_M - \mathbf{v}_a - \mathbf{G}\Delta\mathbf{p}) \quad (7)$$

Minimization of Equation 7 results in determining the change in parameters and sets the variables for the next iteration. The process is complete when the required change in parameters is sufficiently small. The sensitivity matrix plays an important role in ensuring the method is executed properly. In order to determine a unique solution, the number of measured points has to be greater than the number of selected parameters. The selection of parameters has to indicate the appropriate parameter and location of the selected parameter. Improper use of the sensitivity matrix can result in values losing their physical meaning. That is, while a mathematical solution may be possible, the changed parameters will no longer represent reality. Effort must be made to minimize actual parameter changes, and to limit the possible values of selected parameters to reflect reasonable values. Though the model still may lose its physical meaning, care in updating can allow the creation of a more accurate model.

Determining the sensitivity matrix is a crucial step to solving the modal equations. Natke's method uses the modal equations of motion to provide the calculation of updating parameters (Natke 2012). The system matrices are updated according to the following:

$$\mathbf{K} = \mathbf{K}_A + \sum \alpha_i \mathbf{K}_i$$

$$\mathbf{M} = \mathbf{M}_A + \sum \beta_j \mathbf{M}_j \qquad (8)$$

$$\mathbf{D} = \mathbf{D}_A + \sum \gamma_k \mathbf{D}_k$$

$[\alpha_i \ \beta_i \ \gamma_i] = [p_s]$: unknown correction parameters

K_i, M_j, D_k: substructure matrices defining the location and type of modal uncertainty

By defining parameter changes in terms of stiffness and mass, the change in parameters are converted to a change in modal characteristics. Stiffness and mass matrices are available

from SAP. Damping changes are ignored. Defining the sensitivity matrix depends on the method of residual calculation. Residuals are typically defined between eingenvalues and eigenvectors. Both methods are based on an undamped system, so the structure is assumed undamped. The following equations are based on those presented by John Mottershead (Mottershead et al. 2010).

The eigenvalues are defined as the squares of the measured natural frequency. The residuals are defined as the difference between the measured eigenvalues and those determined analytically. The sensitivity matrix is based on the change in the undamped eigenvalues, and can be determined analytically based on Equation 6.

$$\frac{\partial \lambda_j}{\partial \theta_k} = \boldsymbol{\varphi}_j^T \left[-\lambda_j \frac{\partial \mathbf{M}}{\partial \theta_k} + \frac{\partial \mathbf{K}}{\partial \theta_k} \right] \boldsymbol{\varphi}_j \qquad (9)$$

λ represents the eigenvalue for the selected mode (j)

$\boldsymbol{\varphi}$ is the mode shape at the selected mode (j)

$\boldsymbol{\theta}$ is the selected parameter (k)

The eigenvector residuals are the difference between the measured and analytical mode shapes. The comparison is only required at the degrees of freedom determined by the measurement locations. Determining the sensitivity matrix of the mode shapes can be a difficult task. The method defined by Fox and Kapoor is one of the most simple methods and is the one used here (Fox and Kapoor 1968).

$$\frac{\partial \boldsymbol{\varphi}_j}{\partial \theta_k} = \sum_{h=1}^{H} a_{jkh} \boldsymbol{\varphi}_h \qquad (10)$$

The gradient is formed by creating a weighted sum of eigenvectors. After substituting Equation 10 into Equation 9, the factor a_{jkh} is defined as indicated in Equations 11 and 13.

$$a_{jkh} = \frac{\boldsymbol{\varphi}_h^T(-\lambda_j \frac{\partial \mathbf{M}}{\partial \theta_k} + \frac{\partial \mathbf{K}}{\partial \theta_k})\boldsymbol{\varphi}_j}{(\lambda_j - \lambda_h)}; \quad h \neq j \qquad (11)$$

$$a_{jkh} = -\frac{1}{2}\boldsymbol{\varphi}_j^T(\frac{\partial \mathbf{M}}{\partial \theta_k})\boldsymbol{\varphi}_j \qquad (12)$$

These equations can then be placed into the residual equation to determine the required change in parameters. Consecutive iterations of this method will result in the corrected model. Minimizing the objective equation at the current iteration point gives Equation 13, which defines the change in parameters.

$$\mathbf{r}_M - \mathbf{r}_A = \mathbf{G}\Delta\mathbf{p} \qquad (13)$$

$\mathbf{r}_M$: The weighted measured mode shape

$\mathbf{r}_A$: The weighted analytical mode shape

other variables described above.

These equations are described here only briefly, and additional descriptions can be found in the papers mentioned. The calibration of the model was done for the values taken from the first shaker test, and then correlated with the values from the second shaker test to determine the accuracy of calibration.

Chapter 4: Results and Recommendations

Embedded Sensor Effectiveness

The embedded sensors installed in the bridge have the primary goal of detecting the natural frequencies of the structure. Initial attempts to determine the natural frequencies present were unsuccessful and the data detected was determined to be unusable. The typical time history of the sensors would commonly look like Figure 4.1. It was apparent from the recorded values that enough digitization was occurring on the sensors to blot out actual measurements. Digitization is the process of converting an electrical signal into a discrete numerical value. Though the recorded numbers may have precise decimal readings, the values of the numbers are limited to a specific range of values. Campbell Scientific Dataloggers define this as the datalogger's resolution. A CR1000, for example, would be able to measure in increments of 1667 μV (Campbell Scientific 2011). The larger this number, the larger the sensor readings required to be detected. The CR3000 has a higher resolution than the CR1000, of 167μV. As shown in Figure 4.1, this resolution value is also indicated by the measured points. The graph shows the accelerometer's time history response and indicates the exact values that were recorded. Values are rounded to a limited number of specific numerical values.

In order for digitization to have a large impact on data, the variance in the data must be small. Because the accelerometers were embedded in the bridge, it was difficult to diagnose the actual problem, whether the bridge response was actually small or if the accelerometers were malfunctioning. It is possible that the accelerometers were damaged so their output was severely limited, putting the readings below the required threshold for measurement. In order to test the accelerometer's response, sufficient excitation had to be applied to the bridge to excite

acceleration above the current threshold. To confirm the accuracy of any reported readings, an alternative system was used. Both the impact test and the first shaker test were used to calibrate the readings of the embedded accelerometers.

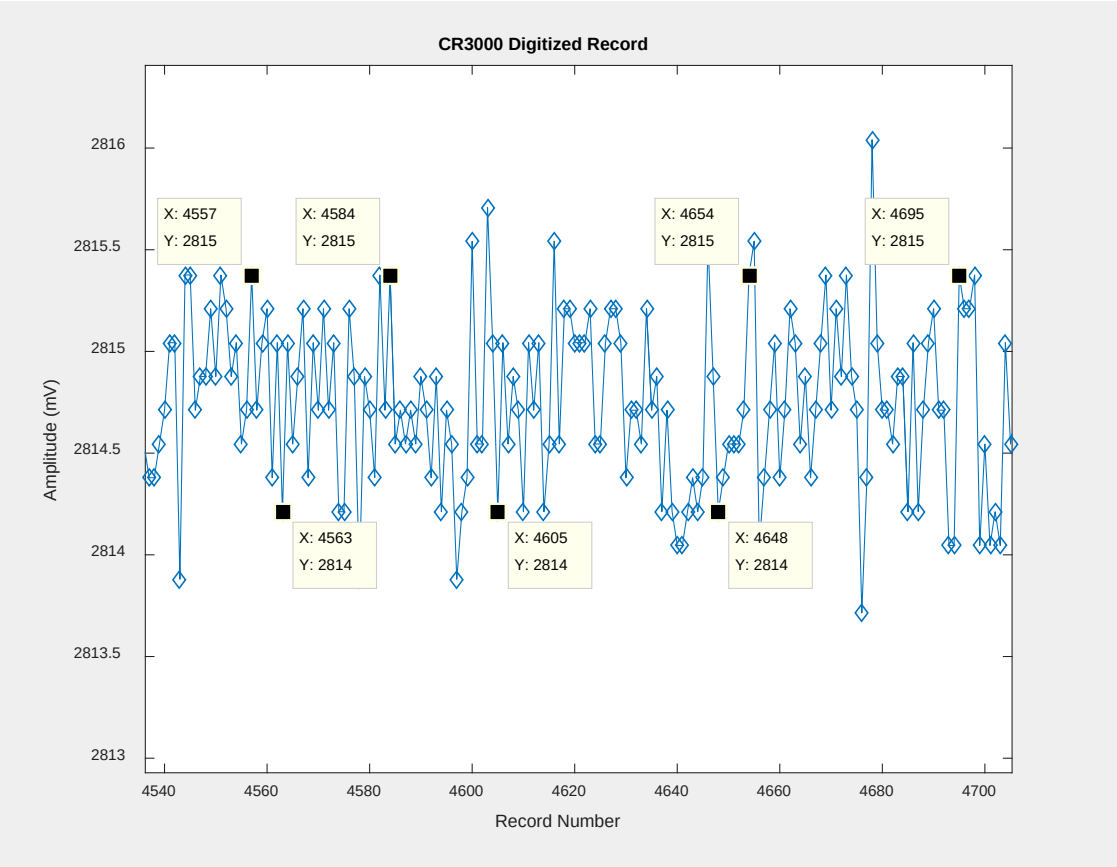

Figure 4.1: A Digitized Signal from the Impact Test using a CR3000

Accelerometers were monitored using a CR3000 during the impact test. Though excitations were too small for the CR3000 to detect under ambient vibration, the impact test promised excitations large enough to read. Velocity transducers with far more sensitivity were placed on the bridge as well, to calibrate the readings of the accelerometers. These two values could be coordinated by differentiation of the velocity transducer readings. Differentiation can be done using Matlab's "diff" function. This function returns the difference between consecutive points along a vector. It is important to remember to include units of time in the solution of this

differentiation. The resulting solution must be divided by the time step between each measured point.

After converting all signals into units of m/s^2, the relative acceleration could be compared. It was assumed that two sensors in a similar location would have similar amplitudes of acceleration. The data from the velocity transducer at the midspan of the central girder (sensor number 4) was noted to be unusable after the test. Interpolation based on the relative amplitudes of the velocity transducers along the side of the bridge were used to calculate and estimated value for the midspan of girder 5. This was compared with other signals to assure a reasonable estimate. Figure 4.2 shows a typical comparison between both sensors.

The peak response values for each impact peak were averaged to determine the response from hitting at each location. Table 4.1 shows the averaged peak response of the accelerometers at each sensor for each hitting location. This table can be compared with Table 4.2, showing the same information for the velocity transducers. Impact locations on girder 1 are located on the northern sidewalk and show a decreased response. Decreased peak response from these locations is similar to a decreased response detected by the velocity transducers. Response can be seen decreasing further away from the impact point.

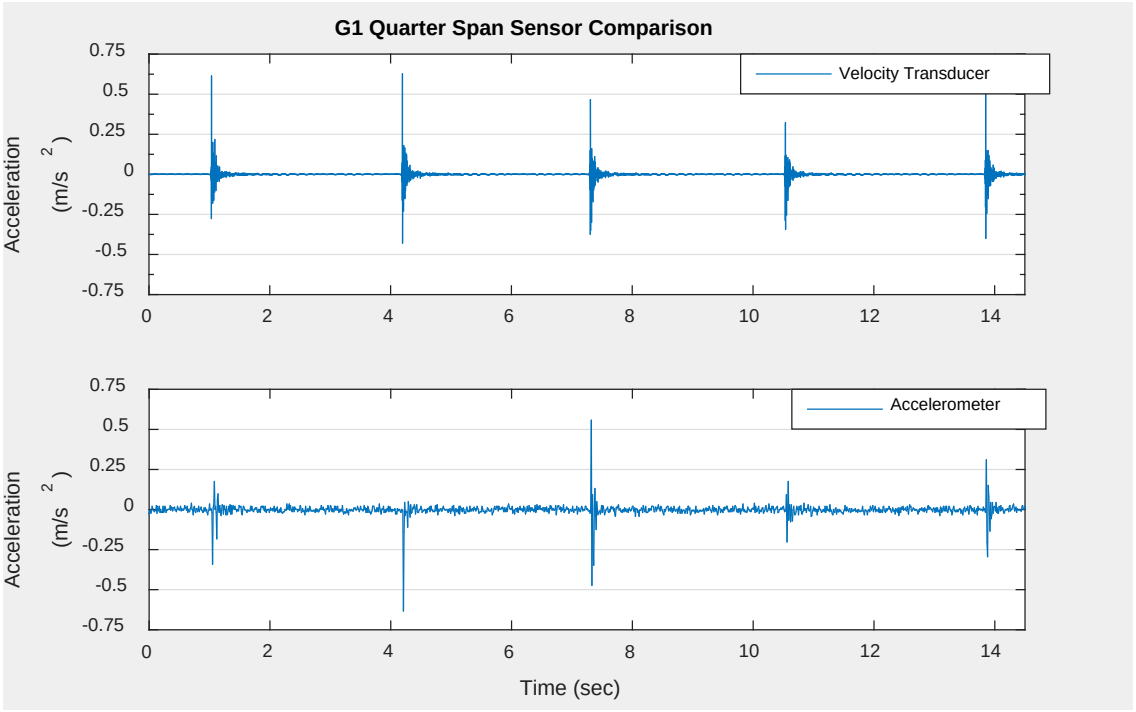

Figure 4.2: Response Comparison of Both Types of Sensors during the Impact Test

Both tables show similar trends in relative amplitudes. Interestingly, the response of the accelerometers at the impact point is lower than the sensor that shares the girder. For example, for impact at girder 1 midspan, the response at girder 1 quarter span is larger than the response at girder 1 midspan. This behavior is shared for each impact point measured by the accelerometers. The velocity transducers do not show this behavior. The largest accelerations occur near the excitation point and decrease farther from the point.

Table 4.1: Average Peak Response by Accelerometers Given Impact Location, in units of m/s^2

Sensor Location	Acceleration at Impact Location (m/s^2)			
	Girder 1 Mid	Girder 1 Quarter	Girder 5 Mid	Girder 5 Quarter
Girder 1 Mid	0.360	0.881	0.165	0.115
Girder 1 Quarter	0.410	0.264	0.205	0.083
Girder 5 Mid	0.159	0.134	0.774	0.584
Girder 5 Quarter	0.148	0.175	0.870	0.749

Table 4.2: Average Peak Response by Velocity Transducers Given Impact Location, in units of m/s²

Sensor Location	Acceleration at Impact Location (m/s²)			
	Girder 1 Mid	Girder 1 Quarter	Girder 5 Mid	Girder 5 Quarter
Girder 1 Mid	0.951	0.500	0.288	0.111
Girder 1 Quarter	0.516	0.930	0.169	0.139
Girder 5 Mid	0.675	0.550	6.419	1.426
Girder 5 Quarter	0.450	0.731	3.210	2.947

Table 4.3 shows the ratio of accelerometer readings to velocity transducer readings, aligned according to impact like the previous tables. A large variation exists between each ratio of acceleration. Table 4.4 shows the average ratio for each accelerometer and the variance between readings. The most consistent ratio was had by the Girder 5 quarter span accelerometer, with a ratio of 0.275 on average. There appears to be no correlation between impact location and sensor ratio. Most readings are below those detected by the velocity transducers.

Table 4.3: Ratio of Accelerometer Response to Velocity Transducer Response

Sensor Location	Impact Location			
	Girder 1 Mid	Girder 1 Quarter	Girder 5 Mid	Girder 5 Quarter
Girder 1 Mid	0.393	0.584	1.064	1.790
Girder 1 Quarter	0.789	1.221	0.606	0.283
Girder 5 Mid	0.237	0.125	0.435	0.259
Girder 5 Quarter	0.332	0.272	0.257	0.240

Table 4.4: Average Ratio of Accelerometers and Velocity Transducers

Sensor Location	Average Ratio	Variance
Girder 1 Mid	0.958	0.388
Girder 1 Quarter	0.725	0.153
Girder 5 Mid	0.264	0.016
Girder 5 Quarter	0.276	0.002

The Girder 5 quarter span accelerometer has the most consistent ratio. Using this value, the acceleration detected by the accelerometers were less than one third that detected by the velocity transducers. The large variability makes any actual accelerometer measurements

questionable. This test is not conclusive, however. The sample rate was very low for an impact test. It is likely that the largest impact was missed by some sensors. Also, the accelerometers were being measured using the CR3000, which has poorer resolution than other dataloggers. However, the results of this test indicate that while the accelerometers are responding, their readings are most likely below the expected value.

Due to the high digitization of the accelerometer readings, they were unusable for determining the power spectrum of the bridge during this test. The embedded sensors were also monitored during the shaker test, however, with a more capable datalogger.

The accelerometers were monitored during the first shaker test using a CR9000. The CR9000 has a much better resolution of 0.01 mV. It also was able to sample at 5000 Hz. This data was able to form a power spectrum of the bridge. However, due to the high noise in the accelerometer readings, the effect of the shaker could only be seen after increasing the amplitude. To confirm the results described above, the peak amplitudes of the velocity transducer and its corresponding accelerometer were compared. The method of comparison is the same for that described above.

Initial correlation between the two sensor types proved difficult due to the high amounts of noise in the accelerometer signal. As shown in Figure 4.3, the actual amplitude of the accelerometer response is debatable. By filtering the high frequency noise from the signal, the steady state could be more accurately compared. It is important to note the high noise amplitude relative to the actual response signal, in that this may cause difficulty for all future signals. Two different filters were tried to determine the most effective one. A simple Butterworth filter was used to remove all frequencies above 25 Hz. This filter was chosen because it functions well as a low pass filter and leaves very little residual of the higher frequencies. Because only

frequencies below the stop band were tested, the loss of higher frequencies will not impact the goal of this test. The larger roll off is also negligible because the noisy frequency is much higher than the stopband of 35 Hz. Also, the phase shift due to filtering could be ignored, as only the peak amplitudes between signals were being compared.

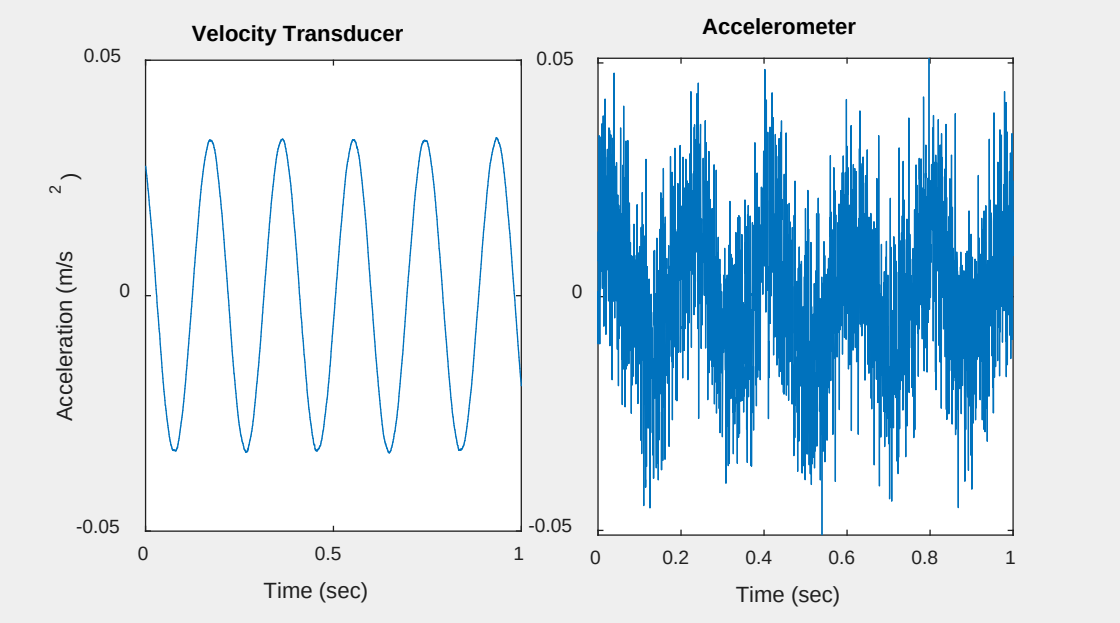

Figure 4.3: The Steady State Response as Recorded by both Sensor types at the Girder 5 Midspan

The second filter used was an Elliptical filter, with the same conditions as indicated for the Butterworth filter. The Elliptical filter has a faster roll off but a larger ripple effect. Both filters were designed using MATLAB's filter design tool. Both filters presented roughly the same result, shown in Figure 4.4. The signal is much smoother than the original, but indicates the difficulty in filtering the signal to match the results given by the velocity transducers.

Both sensors had similar results. The Butterworth filter was chosen due to the reduced ripple effect of the filter. Further results using filters use the Butterworth filter. Both filters show a reduction in amplitude, which is likely completely due to noise. Noise would have less

of an effect during the impact test, where all of the responses were much larger. Using the filtered data, the correspondence between the two signals could be compared, just as done for the impact test. The ratios of averaged peak amplitudes of accelerometers against averaged peak amplitudes of the corresponding velocity transducers are shown in Table 4.5.

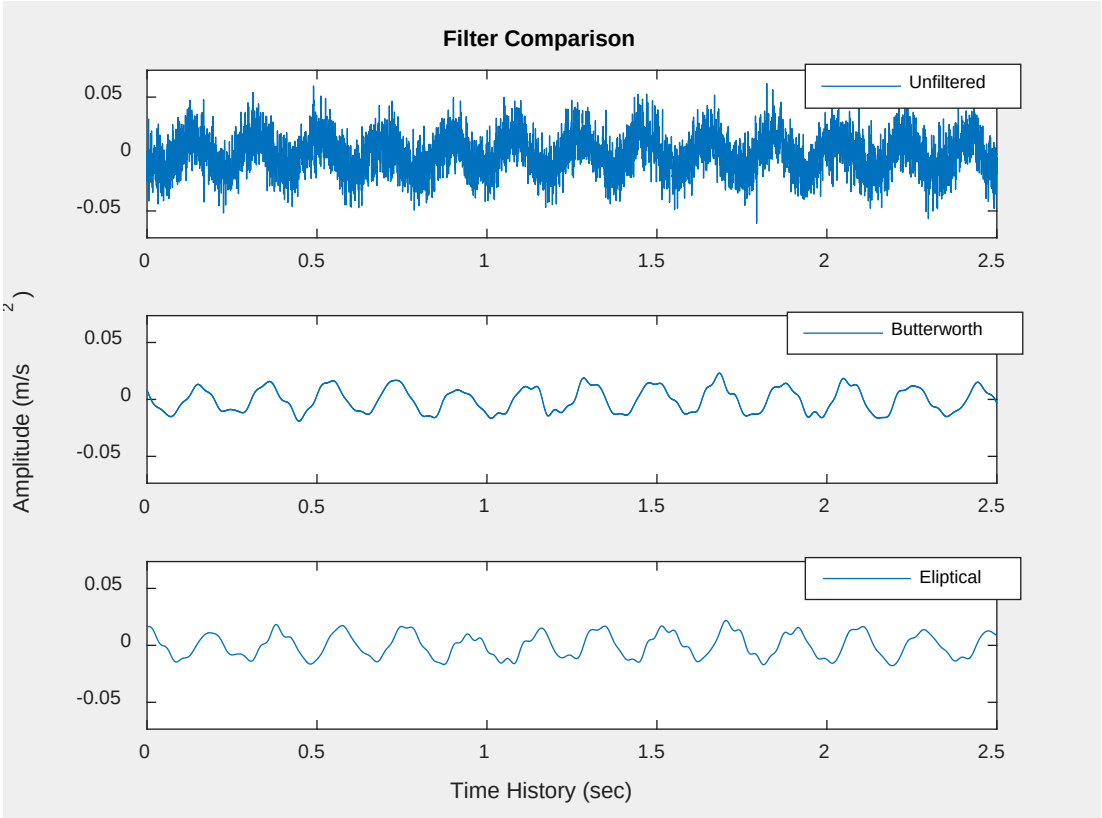

Figure 4.4: A Comparison of the Filtered Signals

Table 4.5: Ratio of Response between Velocity Transducers and Accelerometers at Various Shaker Excitations

Sensor Location	Mode Excited (Excitation Frequency)			
	Mode 1 (5.25 Hz)	Mode 2 (6.20 Hz)	Mode 3 (7.30 Hz)	Mode 4 (8.65 Hz)
Girder 1 Mid	0.987	1.069	1.135	0.998
Girder 1 Quarter	1.070	1.071	1.330	1.059
Girder 5 Mid	0.610	1.001	0.768	0.634
Girder 5 Quarter	1.531	1.871	1.813	1.658

The data recorded during this test, after filtering, has much closer correlation to the response given by the velocity transducers. Though the values still have some variation, the spread of each sensor is much less than those detected during the impact test. The results are generalized in Table 4.6.

The ratio obtained from the shaker test differs significantly from the ratio determined during the impact test. The most likely explanation for this difference is the difference in data collection. 100 Hz is very slow for an impact test, and likely missed the peak points. Unfortunately, there were no other options at the time. The shaker test had no lost data due to data resolution and monitored at a significantly higher sample rate. Also, steady state testing is typically more accurate for amplitude than impact testing. It is the author's opinion that the shaker test results are the most reliable, as the data acquisition system was far superior to that used in the impact test.

Based on the results of these tests, it appears that though the accelerometers are not perfectly aligned with the velocity transducers, they do have an accurate response. At the very least, the sensors are working. It is likely they could be easily used for frequency analysis even with the large noise ratio. They may not have much further use beyond that.

Table 4.6: Results of the Comparison of the Shaker Test

Sensor Location	Average Ratio	Variance
Girder 1 Mid	1.047	.005
Girder 1 Quarter	1.133	.017
Girder 5 Mid	0.753	.032
Girder 5 Quarter	1.718	.024

In the comparison of frequency, it is important to note the difference between the filtered and unfiltered signal. Though the frequency results of the bridge use data from the embedded sensors as well as the velocity transducers, a mention on the value of filtering is made here.

Future use of the sensors will have similar issues with noise, so knowing how filtering effects the results could be valuable.

To demonstrate the difference between the power spectrum for both unfiltered and filtered cases, the shaker test results will be used. The swept sine test, recorded at the second shaker location, was recorded by the dataloggers. The power spectrum, defined by the Pwelch function, is shown in Figure 4.5. As indicated by the figure, no significant difference is noticed between the filtered and unfiltered case. This applies only to the lower frequencies. Higher frequencies show large divergence, as they are completely removed by the filter.

Another issue with the noise ratio is the problem of sufficient excitation. Because the bridge is relatively short and does not experience a high traffic load, the noise generated by the sensors may completely cover actual vibrations from excitation. Ambient vibration during the shaker test indicated that accelerations of 0.03 m/s^2 would be expected by the bridge. Noise observed in the accelerometer signal had a typical range of approximately 0.03 m/s^2, sometimes higher. Basing typical acceleration on the ambient excitation amplitudes on the record of the velocity transducers during the second shaker test, it is possible that the noise level in the embedded accelerometers would exceed that created by the excitation of a vehicle crossing the bridge. Additional tests would be needed to determine the effectiveness of the accelerometers under ambient excitation.

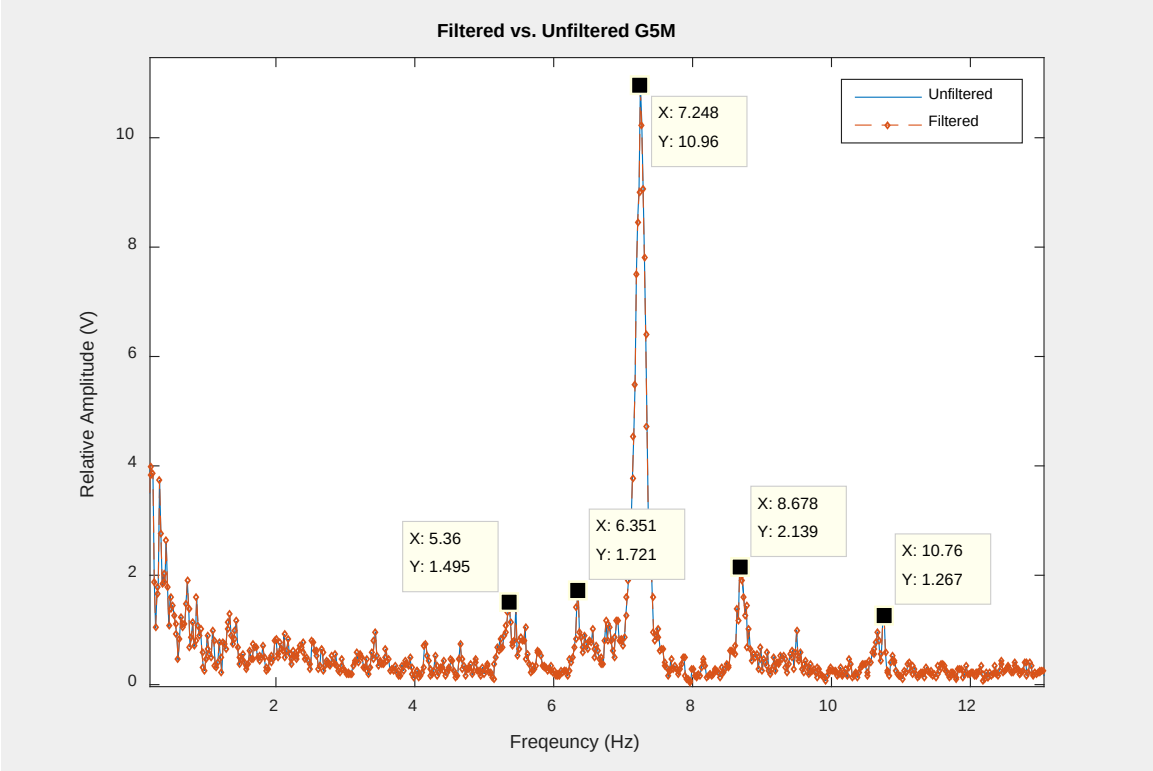

Figure 4.5: Comparison of the Power Spectrum for Filtered and Unfiltered Accelerometers

Modal Frequency Changes

The modal frequencies of the bridge were recorded for each of the three tests. The frequencies were detected using the power spectrum. The comparison of the frequencies between tests will indicate the change in frequency due to various changes in the bridge. Also, these tests establish the expected frequencies of the bridge. This lays the groundwork for future studies and correlations. The first five modes were the primary focus of these tests and are the only ones reported.

The impact test performed on June 29th was done before the asphalt was placed on the bridge. The modal frequencies were detected using the data physics system. The embedded sensors had poor recorded data and were not useable for determining the modal frequency.

A power spectrum is shown in Figure 4.6 for the two sensors placed on girder 1, sensors 1 and 2. As would be expected, the relative amplitude of the more central placed sensor is larger than the amplitude of sensors placed closer to the edge of the bridge. Using power spectrums like these, the modal frequencies can be determined. The modal frequencies detected by each sensor are indicated in Table 4.7. Sensor 4's data was corrupt, and is thereby not included.

The two middle sensors, numbered 3 and 7, had no revealing spike at the second mode. This was due to the location of the sensors. The sensors were placed at the center of the bridge, where the node for the second mode was located. This aids in confirming the mode shape of the second mode.

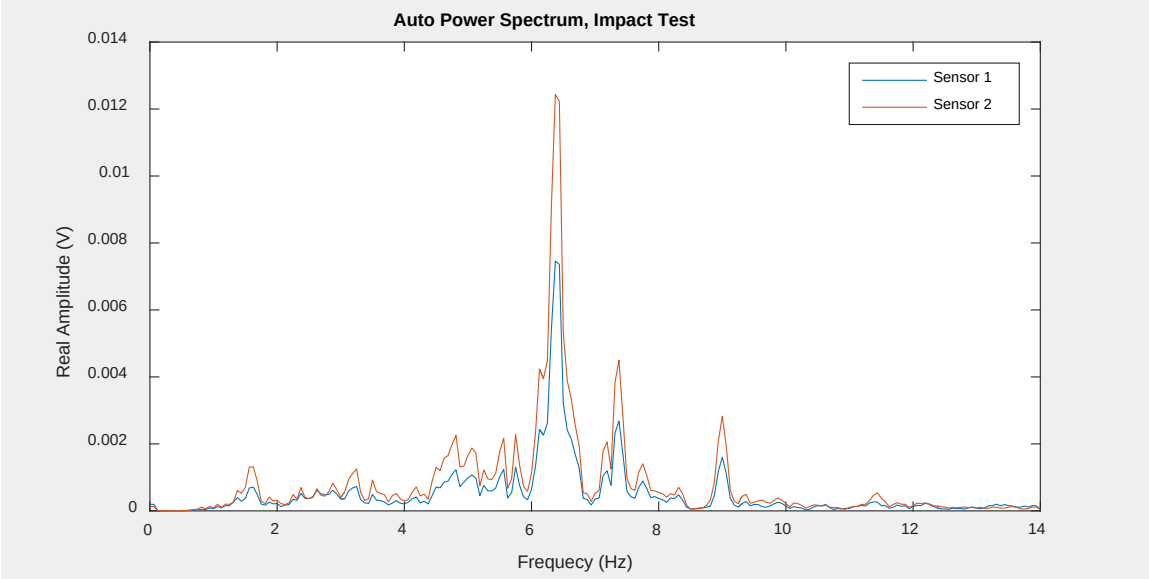

Figure 4.6: The Power Spectrum for the Impact Test

Table 4.7: Frequencies Detected during the Impact Test

Sensor	Mode 1 (Hz)	Mode 2 (Hz)	Mode 3 (Hz)	Mode 4 (Hz)	Mode 5 (Hz)
1	5.62	6.5	7.25	8.94	11.25
2	5.62	6.5	7.25	8.94	11.25
3	5.62	-	7.25	8.94	11.25
5	5.62	6.5	7.25	8.94	11.25
6	5.62	6.5	7.25	8.94	11.25
7	5.62	-	7.25	8.94	11.25

The shaker test had similar results. The natural frequencies of the bridge were primarily detected during the swept sine tests run on the bridge. The frequencies detected were somewhat dependent on where the shaker was located. Table 4.8 shows the frequencies detected for the first shaker position. The second shaker test indicated another large peak at 9.4 Hz. This frequency was subsequently investigated and may represent the fifth mode shape, which was likely more easily excited by the edge location of the sensor.

Table 4.8: Frequencies Detected during the First Shaker Test

Sensor	Shaker Position 1 Mode Frequencies (Hz)				
1	5.33	6.29	7.21	8.56	10.57
3	5.35	6.29	7.21	8.56	10.57
6	5.35	6.29	7.23	8.59	10.54
8	5.35	6.29	7.25	8.59	10.54
9	5.37	6.27	7.25	8.56	10.55
11	5.37	6.27	7.25	8.56	10.55

Comparisons between the two tests indicate the difference between the bridge before and after placement of the asphalt. Typically, the additional mass of the asphalt would cause the natural frequencies to decrease. Using the averages taken from each test, the comparison between the frequencies could be made. Because modal frequency values are very similar between all sensors for both tests, the values appear to be very accurate. The comparison between the two tests is shown in Table 4.9. The ratio of frequency change depends on which

mode is being observed. The parameter change in the structure was due primarily to the additional mass of the asphalt. As indicated by Morassi (2008), a parameter change of the structure has the most effect on those modes that have the most motion in the area where the change occurs.

In this case, modes with less motion across the bridge center will be influenced less by the additional asphalt. The third mode shape has most of its motion in the sidewalk, and two nodes in the asphalt region. Modes four and five also have nodes in the asphalt region, but these modes have additional movement across that area. The mode shapes are shown visually in the last section of this chapter.

Table 4.9: Comparison of the Shaker and Impact Tests

Mode	Impact Test (Hz)	Shaker Test (Hz)	Difference	Ratio
1	5.62	5.35	0.27	0.95
2	6.50	6.29	0.21	0.97
3	7.25	7.23	0.02	0.99
4	8.94	8.57	0.37	0.96
5	11.25	10.55	0.70	0.94

Another aspect to consider is the effect of temperature on the structure. Temperature can affect the natural frequency, but the nature of the effect is dependent on the structure. For thorough consideration, though, the temperature recorded in the bridge on the day of the impact test can be considered as a variable. Selecting an inclusive temperature for the bridge at the time of the test can be difficult. This issue is explored here since future monitoring must address this problem.

The variation in temperature exists in all three dimensions across the bridge. The vertical variation is defined primarily by the amount of solar radiation heating the bridge. The spread between upper and lower thermocouples is greatest during the days on the hottest months of the

year, peaking near the summer solstice. The lowest variance occurred at night, where all temperatures approached equal values. North-South temperature gradients had a similar variation. Those sensors beneath the asphalt had higher peak temperatures, while those beneath the sidewalk changed temperature more slowly due to the insulation of the sidewalk. Variation in the East-West direction was minimal, but the central thermocouples typically had higher temperature, though this was not a consistent variation. To account for this variation, the method involved comparing averages vertically and then horizontally across the girder. First, the thermocouple readings were averaged, representing the average near the top of the girder. This was then averaged against the temperature readings from the strain gauges, giving an average at that point on the girder. Averaging this value with all points on the girder gave a girder average. Finally, the temperature used was the average of both girders. The determined temperatures are shown in Table 4.10.

At the time of the impact test, girder 1 had a top average temperature of 31ºC and girder 5 had a top average temperature of 36ºC. The temperature at the bottom of the girder remained near 25ºC for both girders. The first shaker test was done over a long time period, including a range of temperatures. Part of the test occurred in the morning, where the average temperature for most sensors remained around 20ºC. Temperature began to increase in the afternoon, and the centrally located sensors increased to up to 40ºC, while those below the sidewalk had a very small increase in temperature. The detected frequencies were based on a specific swept sine test, so the temperature is based on the hour that test took place. This process was also used during the second shaker test. However, throughout each test the dynamic properties were likely changing slightly due to changing temperature gradients.

Table 4.10: Temperature of the bridge at the time of each test

Test	Temperature (°C)
Impact	31
1st Shaker	23
2nd Shaker	5

The temperature within the bridge during the second shaker test was averaged to be 5ºC. The temperature remained within a few degrees Celsius throughout the test. This represents roughly an 18ºC difference between the first and second shaker tests.

The second shaker test indicated a slight change in natural frequencies. The results for the sensors in the same locations as those indicated in the above tests are shown in Table 4.11. As in the first shaker test, the seventh sensor had poor results. Although the sensor did show a clear response, the response had low amplitude and was out of phase with its neighbors. The value was unusable for modal criterion, but still gave reliable results in the frequency domain.

A special note must be made on the values indicated for mode 5. In swept sine tests, the mode was unnoticeable on the power spectrum. The data of Table 4.11 was confirmed using the ambient data taken during the shaker test. The fifth mode was determined using this data, as the mode was visible on those power spectrums. An example of the power spectrum for the swept sine test and the ambient test is shown in Figure 4.7. An explanation for this was found by reviewing the experiment layout. Using the finite element model, the fifth mode has nodes located near 1.83 m (6 ft) and 6.4 m (21 ft) from the north edge. These were the locations chosen to excite the bridge. The fifth mode shape, and natural frequency, likely weren't being excited by the shaker. Unfortunately, this was not visible on many of the power spectrums viewed during the test because traffic provided almost continual ambient excitation.

Comparing each of the three tests, a description of the power spectrum of the bridge can be defined, even if somewhat loosely. The values from all three tests are shown in Table 4.12.

Table 4.11: The Frequencies Detected during the Second Shaker Test.

Sensor	Mode 1 (Hz)	Mode 2 (Hz)	Mode 3 (Hz)	Mode 4 (Hz)	Mode 5* (Hz)
1	5.39	6.48	7.46	9.18	11.88
2	5.39	6.48	7.46	9.18	11.84
7	5.35	6.33	7.50	9.18	12.30
8	5.35	6.41	7.54	9.22	11.84
13	5.43	6.41	7.54	9.18	11.84
14	5.43	6.41	7.54	9.18	11.84

**Mode 5 values were based only on ambient vibration.*

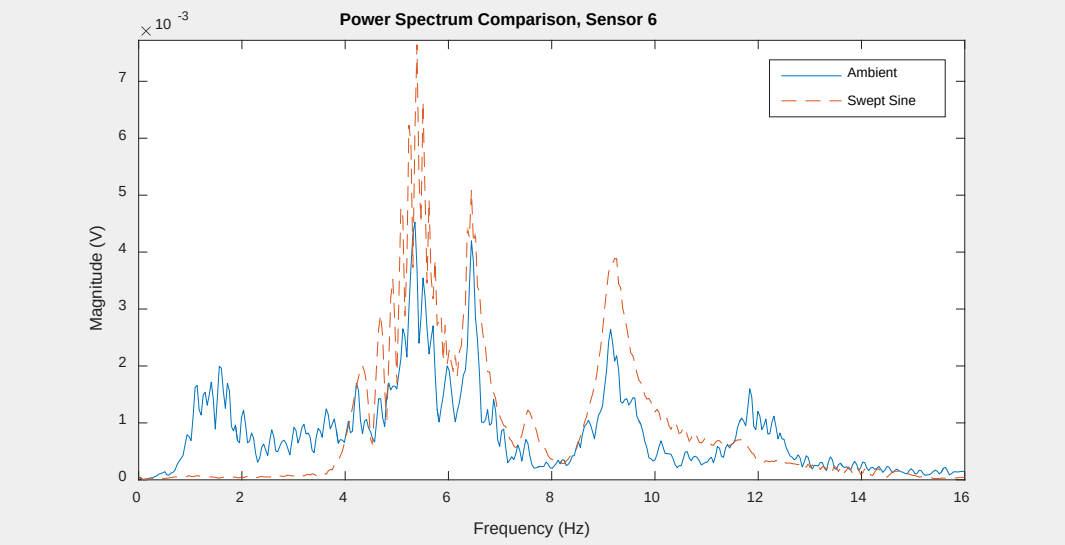

Figure 4.7: Comparison of the Power Spectrum Returned using Ambient and Swept Sine Excitation

Table 4.12: Modal Frequencies Detected during Each Test

Test	Mode 1 (Hz)	Mode 2 (Hz)	Mode 3 (Hz)	Mode 4 (Hz)	Mode 5 (Hz)	Temperature (°C)
Impact	5.62	6.5	7.25	8.94	11.25	31
First Shaker	5.35	6.29	7.23	8.57	10.55	23
Second Shaker	5.39	6.42	7.51	9.19	11.85	5

The change in temperature between shaker tests appears to have correlated to an increase in the frequency of each mode. This follows typical convention, with decreased temperature

resulting in increased stiffness, thus raising the frequency. A comparison of the frequencies detected during the two tests is shown in Table 4.13. The change in modal frequency is greater for higher modes. The result suggests that temperature effects will have a more noticeable impact on higher mode frequencies than lower mode frequencies. Thus, in detecting frequency changes due to temperature, detecting higher modes appears to be more precise. Since higher modal frequencies are also more affected by damage, being able to correlate temperature and higher modes can provide a more useful baseline than if lower modes are used. However, additional testing is required to confirm these preliminary results.

Finite Element Modeling Results

The initial finite element model was selected from multiple options based on a good MAC correlation. The various models included additional sections defining the sidewalk and parapet, initially changing the spring stiffness, and changes to overall stiffness. The selected model had the initial MAC values shown in Table 4.14. Correlation was performed between the model and the measured values from the first shaker test. The initial correlation shows some oddities between many mode shapes that are not the same. In fact, the correlation between mode 1 and mode 5 is higher than the correlation between mode 1 and itself. This correlation occurs due to the low number of measurement locations. Orthogonality is based on the displacement of all degrees of freedom, but the MAC analysis compares only those degrees of freedom for which values have been measured. In an attempt to improve the correlation, the principle of symmetry was used in this case. Assuming the bridge is symmetrical around the centerline, measurements on one side can be copied to the unmeasured locations on the other side. The Nibley Bridge is

almost completely symmetric, aside from the sewer pipe that passes between girders 3 and 4. This method is used to increase the accuracy of the final MAC analysis shown later.

Table 4.13: Frequency Comparison between First and Second Shaker Test

Mode	1st Shaker Test (Hz)	2nd Shaker Test (Hz)	Difference	Ratio
1	5.35	5.39	0.04	0.99
2	6.29	6.42	0.13	0.98
3	7.23	7.51	0.28	0.96
4	8.57	9.19	0.62	0.93
5	10.55	11.85	1.30	0.89

Determining the mode shapes defined by testing involved matching the excitation frequency to a mode shape and waiting for the system to reach steady state. After steady state was reached, if the responses were in phase or 180° out of phase, then it was determined the system was vibrating at a specific mode. This method isn't perfect because noise, measurement errors, and additional excitation all result in imperfect data. The steady state response at the second mode is shown in Figure 4.8. The mode shapes are seen to fit the criterion for a modal response. The data from the shaker has a noteworthy difference from the finite element data. Examining two measurement locations that are equally spaced from the center of the bridge, the peak amplitudes should be equivalent. In Figure 4.8, sensors 3 and 11 are both placed at the center of the outside girder. Ideally, these sensors would both have the same amplitude. However, it was observed that the farther a sensor was from the shaker, the greater decrease in amplitude it would have relative to its corresponding sensor. A few methods to correct for this were proposed in Link's paper (Link 2000). The method involves adjusting the measured values to more fully reflect the analytical values by applying a correction factor. This method is considered to be applied after parameter updating has taken place. In the case of this paper, the

amplitudes reported by the sensors were used for most cases. The only adjustment was made during the analysis involving the second shaker test.

Table 4.14: Initial MAC Values Based on the First Shaker Test

	Mode 1	Mode 2	Mode 3	Mode 4	Mode 5
Mode 1	0.79	0.03	0.03	0.01	0.80
Mode 2	0.04	0.91	0.00	0.73	0.04
Mode 3	0.36	0.00	0.97	0.03	0.35
Mode 4	0.00	0.82	0.09	0.99	0.00
Mode 5	0.96	0.10	0.26	0.01	0.96

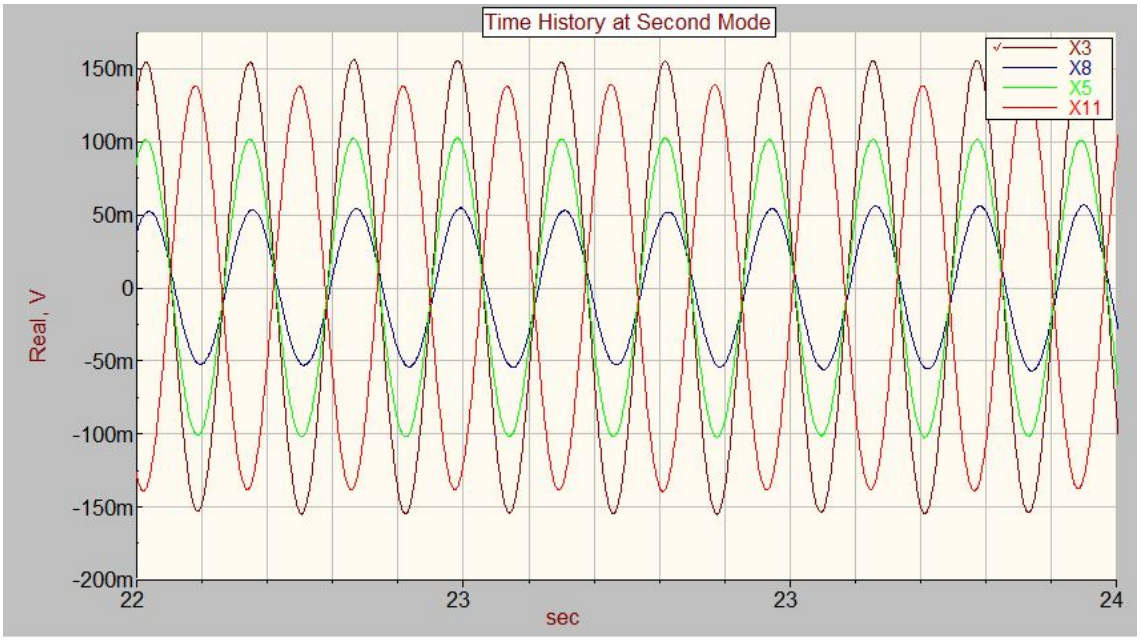

Figure 4.8: An Example of the Steady State Response at a Modal Frequency

Updating of the model required the selection of various updating parameters. Seven parameters were selected based on their ability to influence the mode shapes. The parameters included the Young's Modulus of the beams and deck, as well as the Modulus of the sidewalk and parapet. The rotational and translational stiffness of the spring restraints were each a parameter. The concrete mass density, ρ, for both the sidewalk and the beams and deck was considered. And lastly, the additional mass from the asphalt was considered.

To determine the sensitivity matrix, the change in modal characteristics due to a change in parameters had to be determined. This was done by changing the values of the current model parameters by roughly 10%. This value was selected based on the recommendation by Mottershead's study (Mottershead et al. 2011). The corresponding stiffness and mass matrices were then compared against the original matrices to determine the change due to a single parameter change. These values were then used in the equation to determine the sensitivity matrix as described in chapter 3.

The sensitivity matrix reports which parameters influence the mode shapes the most. Knowing which parameters effect the mode shapes the most can help the designer in determining which shapes should be changed and which should be ignored. A goal of having MAC values above 90% for all modes was decided on before updates occurred. Fortunately, the model quickly reached this goal, because primarily only mode one was below the required tolerance.

Table 4.15 shows the change in parameter values between the first model and the last one. The changes made were based on those values that had the largest effect on the modal properties of the model. The updated MAC values are shown in Table 4.16. Even by adding additional measured points using the bridge symmetry, the mode shapes were very similar. During the second shaker test, additional sensors were used to more fully define the mode shapes, and this similarity is removed from the MAC analysis done using those measurements. Modes one and five as well as modes 2 and 4 are very similar based on the points that were measured during the test.

The largest changes in the model were the spring values, which changed by many factors of ten. After observing the initial guesses for springs, the model was assumed to be incorrect. Translational stiffness was far higher than would be expected reasonably. Spring stiffness also

appeared low, being almost half that recommended by CSI, as indicated in chapter 3 (Kalny 2014). These values were initially adjusted to bring the values closer to realistic bounds. Throughout the modeling process, values had to be corrected to ensure they remained within reason. For example, an asphalt mass of 70 pounds per square foot changes the first mode to very closely align, but that would require approximately six inches of asphalt, and is unreasonable. The author is satisfied that the resulting values are within reason and allow a decent convergence with the determined mode shapes.

Table 4.15: Original and Final Parameter Values for the Model

Parameter	Initial Model Values	Final Model Values	Change
E for Beams and Deck KPa (ksi)	36.2E+6 (5255)	35.8E+6 (5200)	-0.4E+6 (-55)
E for Sidewalk and Parapet Kpa (ksi)	27.6E+6 (4000)	32.4E+6 (4700)	4.8E+6 (700)
Asphalt Additional Mass kg/m^2 (lb./ft^2)	0 (0)	193.2 (39.6)	193.2 (39.6)
Mass Density of Beams and Deck kg/m^3 (lb./ft^3)	2403 (150)	2563 (160)	160 (10)
Mass Density of Sidewalk and Parapet kg/m^3 (lb./ft^3)	2403 (150)	2243 (140)	-160 (-10)
Translational Spring Stiffness KN/m (kip/in.)	43.8E+6 (250E+3)	583.7E+3 (3333)	-43.22E+6 (-246.7E+3)
Rotational Spring Stiffness KN·m/rad (kip·in./rad)	5.65E+6 (50E+6)	6.10E+9 (54.0E+9)	6.09E+9 (53.5E+9)

Table 4.16: Calibrated MAC Values from First Shaker Test

	Mode 1	Mode 2	Mode 3	Mode 4	Mode 5
Mode 1	0.93	0.00	0.00	0.00	0.96
Mode 2	0.00	0.99	0.00	0.70	0.00
Mode 3	0.02	0.02	0.97	0.02	0.01
Mode 4	0.00	0.67	0.02	0.98	0.00
Mode 5	0.95	0.01	0.12	0.01	0.93

Once the model was calibrated, it was then tested against the second shaker test. Some mode shapes were modified from the original data of the second shaker test, specifically in the second and fifth mode shapes. The second mode shape had three sensors, 8, 9, and 10, which were partially out of phase. It appears that at least part of the third mode is affecting the center of the bridge in this data. For the ideal mode, sensor 9 would have zero detected motion. In these results, sensor 9 crosses zero when the other values peak. The image can be seen in Figure 4.9.

To correct these values from the center of the bridge, the values recorded at the in phase position of the other sensors was used. These values were likely closer to the actual modal values. Similar correction was done for the fourth mode, where again the central sensor was out of phase and not near to the expected value for this sensor. The fourth mode also had abnormally high results from sensors 11 and 12. These two values are near zero on the model, and the corresponding sensors, 3 and 4, are both near zero as well.

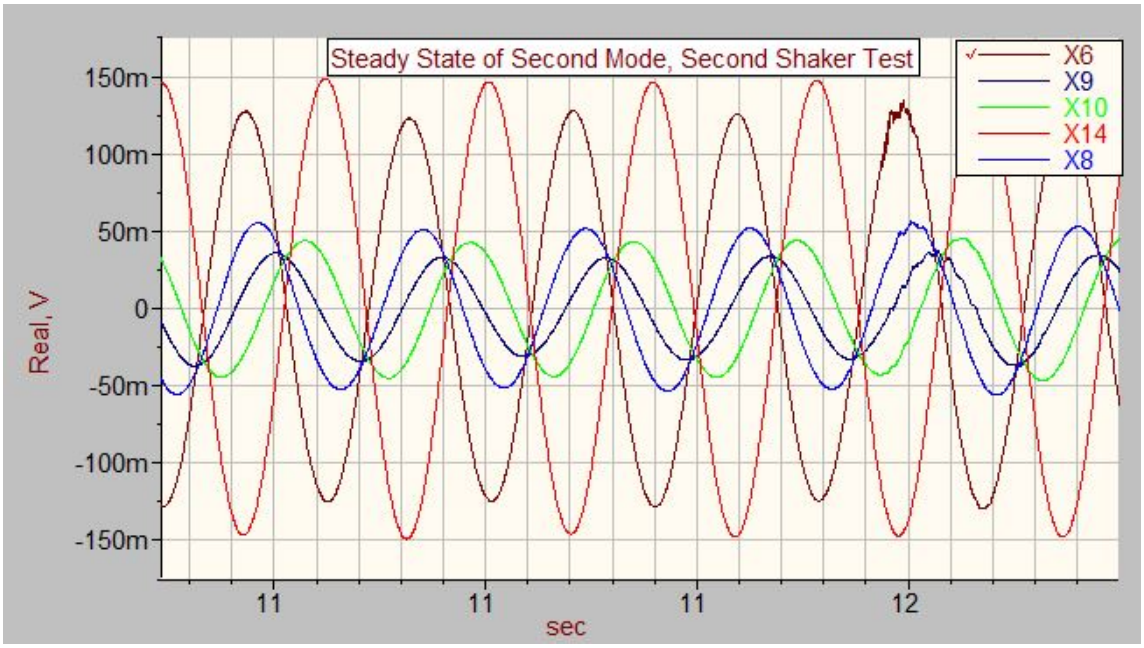

Figure 4.9: Second Mode Steady State Response

As mentioned above, the location of the shaker during the second shaker test was likely on a node of the fifth mode. Due to the shaker's position, the mode was improperly excited, and the response doesn't represent the actual mode shape. A time history of the fifth mode is shown in Figure 4.10. The improper shaker location made this mode difficult to find. The value was only lightly shown on the power spectrum, and the closest steady state had obvious values from another mode in it. Likewise, sensors on the same girder had different directions. The response at this mode, which was found at 12.45 Hz, seems to match more closely with the ninth mode determined by the finite element analysis. For the purposes of the MAC comparison, this mode was ignored, so only the first four modes are used.

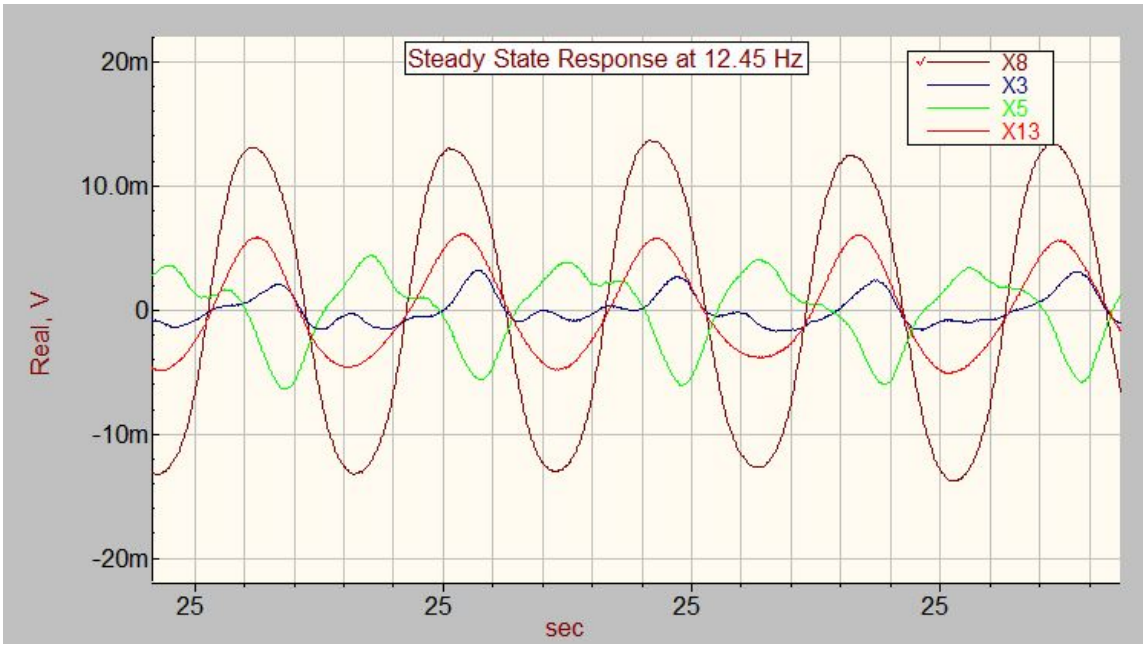

Figure 4.10: Steady State Response near Fifth Mode

The final mode comparison is shown Table 4.17. This correlation does well on the modes detected. More conveniently, this test had additional sensors placed laterally, so a good MAC result is more accurate than the first test would be. Unfortunately, the test data was not as clear as the first data.

The mode shapes indicated by the finite element analysis are shown below in Figure 4.11. Though the mode shapes aligned well with the measured values, the frequencies determined by analysis were not as similar. The frequencies for the first five modes, as determined by the analytical model, are shown in Table 4.18.

As an aside, a MAC comparison between the first and second shaker tests was done. These values, shown in Table 4.19, indicate the similarity between the detected modes between the two tests. As indicated by these values, the fifth mode has very little correlation due to it not being detected on the second test. The other detected modes appear to be the same mode. There were only five sensors placed at the same location between the two tests, so the MAC includes

very few degrees of freedom. This reduced number of degrees of freedom cause the modal pairs, modes one and five and modes two and four, to have high MAC values as well.

Table 4.17: MAC Analysis for the Second Shaker Test

	Mode 1	Mode 2	Mode 3	Mode 4
Mode 1	0.9173	0.1566	0.0182	0.0416
Mode 2	0.0510	0.9673	0.0087	0.0220
Mode 3	0.0048	0.0475	0.9405	0.0003
Mode 4	0.1547	0.1635	0.0169	0.8927

Table 4.18: Modal Frequencies defined by Model

Mode	Frequency (Hz)
1	5.86
2	6.04
3	6.39
4	7.27
5	8.96

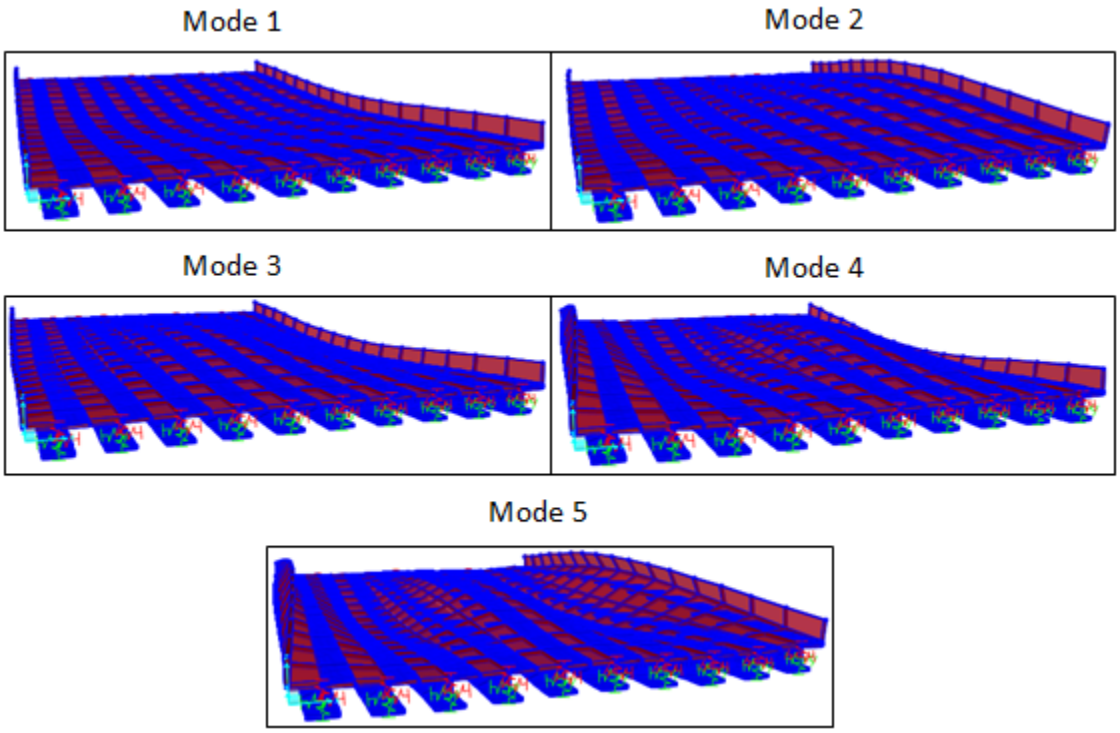

Figure 4.11: Analytical Mode Shapes of Corrected Model

Table 4.19: MAC Analysis for Both Shaker Tests

	Mode 1	Mode 2	Mode 3	Mode 4	Mode 5
Mode 1	0.84	0.01	0.00	0.14	0.21
Mode 2	0.26	0.99	0.06	0.65	0.39
Mode 3	0.03	0.03	0.99	0.00	0.08
Mode 4	0.00	0.74	0.00	0.99	0.89
Mode 5	0.93	0.04	0.11	0.04	0.06

Chapter 5: Summary and Conclusion

The Nibley Bridge has been outfitted with sensors for long term dynamic and strain monitoring. Multiple tests were performed on the Nibley Bridge to establish the dynamic characteristics for future tests. The tests resulted in determination of the natural frequency of the bridge, the corresponding mode shapes, and the effectiveness of the embedded accelerometers.

The embedded accelerometers are reliant on the correct datalogger to operate properly. Using the CR9000, an acceptable sampling frequency and resolution are possible. The only other datalogger that may be sufficient for the site is the CR6. The embedded accelerometers were determined to be operational but suffering from high noise values and low detected amplitudes. Ultimately, the embedded sensors may be useful for detecting the natural frequencies of the bridge, but are inaccurate for other purposes. Filtering the recorded data only affects the higher frequencies, so it is not necessary for low frequency detection. This was confirmed by comparing a power spectrum of both filtered and unfiltered data.

The first five modal frequencies were detected during each test. Over the course of the test, frequency changes were observed due to changes applied to the structure. The changes were caused by the placement of asphalt on the bridge and a change in temperature. The change in frequency was dependent on the mode. The additional asphalt lowered all of the detected frequencies. Frequencies seemed to be effected by this addition depending on how the additional mass affected the mode shapes. Those modes with more movement in the affected area had a greater change in frequency. The third mode changed the least, with a change of only 0.02 Hz. The largest change was in mode five, with a change of 0.70 Hz. Each of the changed frequencies had a ratio greater than 0.94 between pre and post asphalt conditions.

The decrease in temperature caused the detected frequencies to increase. The frequency changes increased with each successive mode. The lowest two modes experienced the lowest frequency change, while the fifth mode changed by more than a hertz. The changes are likely based on how the increased stiffness affects each mode. It is important to note that the higher modes showed the largest sensitivity to temperature change. This indicates that it is important to detect as high of modes as possible when defining frequency changes due to temperature. It may be possible to create a more accurate temperature-frequency baseline using the higher modal frequencies. Since higher modes are also more sensitive to damage, it is important to detect as high of modal frequency as possible.

For this study, the frequency changes matched what would be predicted based on the parameter changes. The detected modal frequencies were near 5.35 Hz, 6.29 Hz, 7.23 Hz, 8.55 Hz, and 10.55 Hz.

The mode shapes were modeled using SAP2000. The finite element model was then calibrated to match the mode shapes detected during the measured tests. The model was changed to make the spring stiffness more realistic. Other changes included changing concrete weights by 160 kg/m^3 (10 lbs/ft^3). Also, the stiffness of the sidewalk and parapet were increased by 4.8E+6 KPa (700 ksi). This change was deemed reasonable since the stiffness began fairly low for concrete. The adjusted parameters were able to match closely the data detected by the second shaker test. MAC results for both tests are almost all above 0.9, indicating that the model accurately represents the mode shapes detected during the tests.

For future testing, it is recommended that a long term correlation between the temperature and frequency of the bridge be established at the highest modes possible. Further study could also be done on how to define the temperature of the structure. By comparing the

temperature gradient effects on the finite element model, a possible solution for the correlation between temperature and frequency may be established. Since the bridge is not held at a uniform temperature, defining the temperature by more than a single value may be useful in calibrating frequencies and temperatures. Since frequency tends to have such a range of values at a single temperature, defining the temperature characteristics of the structure more exactly may improve the correlation between the two values.

Chapter 6: References

Alampalli, S. (1998). "Influence of in-service environment on modal parameters." *In Proc. IMAC XVI,Santa Barbara, CA, pp. 111–116.*

Allenmang, R. J. (2003). "The Modal Assurance Criterion- Twenty Years of Use and Abuse." *Sound and Vibration, August 2003.*

Campbell Scientific. "Training Manual." Campbell Scientific, Inc. Revision 7/11.

Chopra. A.K. (2012). *Dynamics of Structures,*4th Edition. Prentice Hall, New Jersey.

Doebling, S. W. & Farrar, C. R. (1997). "Using statistical analysis to enhance modal-based damage identification." *In Proc. DAMAS 97: structural damage assessment using advanced signal processing procedures, University of Sheffield, UK, pp. 199–210.*

Fox, R. and Kapoor, M. (1968). "Rate of change of eigenvalues and eignevectors." *AIAA J., Vol. 6, pp. 2426-2429*

Faust, N. (2014). *Statistical Models of the Lambert Road Bridge: Changes in Natural Frequencies due to Temperature.* Utah State University, Utah.

Hamed, E., and Frostig, Y. (2006). "Natural Frequencies of bonded and unbonded prestressed beams-prestressed force effects." *J. sound Vib., 295(1-2), 28-39.*

Hsieh, K. H., Halling, M. W., Barr, P. J. (2006). "Overview of Vibrational Structural Health Monitoring with Representative Case Studies." *Journal of Bridge Engineering, 11(2), 707-715.*

Kalny, O. (2014). "Ridgid Behavior." *CSi Knowledge Base.* Web. <https://wiki.csiamerica.com/display/kb/Rigid+behavior> 02 Jan 2017.

Link, M. (2001). "Updating of Analytical Models – Review of Numerical Procedures and Application Aspects." *Structural Dynamics 2000.*

MathWorks. (2016). "Documentation: Pwelch." <https://www.mathworks.com/help/signal/ref/pwelch.html> Web. 29 Dec. 2016.

Morassi, A., Tonon, S., (2008). "Dynamic Testing for Structural Identification of a Bridge." *J.Bridge Eng., 2008, 13(6): 573-585.*

Mottershead, J. E., Link, M., Friswell, M. I. (2010). "The sensitivity method in finite element model updating: A tutorial." *Mechanical Systems and Signal Processing 25 (2011) 2275-2296.*

Natke, H.G., Cempel, C. (2012). "Model-Aided Diagnosis of Mechanical Systems: Fundamentals, Detection, Localization, Assessment." *Springer Science & Business Media.*

Peeters, B., Maeck, J., DeRoeck, G. (2001). “Vibration-based damage detection in civil engineering: excitation forces and temperature effects.” *Smart Mater. Struct. 10 (2001) 518-527.*

Smith, Julius O. III. (2011). *Spectral Audio Signal Processing.* W3K Publishing.

Sohn, H. (2007). “Effects of environmental and operational variability on structural health monitoring.” *Phil. Trans. R. Soc. A. 365, 539-560*

Weisstein, Eric W. (2017). "FourierTransform." *MathWorld*. Web. <http://mathworld.wolfram.com/FourierTransform.html> 16 Feb. 2017.

Welch, P. D. (1967), 'The use of Fast Fourier Transform for the estimation of power spectra: A method based on time averaging over short, modified periodograms", *IEEE Transactions on Audio and Electroacoustics, AU-15 (2): 70–73*

Zhou, G. and Yi, T. (2014). “A Summary Review of Correlations between Temperatures and Vibration Properties of Long-Span Bridges.” *Hindawi Publishing Corporation*: *Mathematical Problems in Engineering, Vol.2014.*